PLASMA ETCHING FOR ADVANCED POLYMER OPTICAL DEVICES

By

DONALD S. BITTING

A DISSERTATION PRESENTED TO THE GRADUATE SCHOOL
OF THE UNIVERSITY OF FLORIDA IN PARTIAL FULFILLMENT
OF THE REQUIREMENTS FOR THE DEGREE OF
DOCTOR OF PHILOSOPHY

UNIVERSITY OF FLORIDA

2003

Copyright 2003

by

Donald Stephen Bitting

Dedicated to my wife, Christine; to my daughter, Kaitlyn; and my family.

ACKNOWLEDGMENTS

This dissertation is a culmination of years of knowledge gained through my experiences in both university and industry. Along the way, I have been fortunate enough to work and learn from many highly accomplished individuals. There are a few of them who stand out in my mind. The following people have gone out of their way to assist me and have been mentors in my life.

In my early years with AT&T Microelectronics, Al Williams and Greg Jones were influential role models for me. They taught me about silicon microfabrication and provided a positive example for the profession of engineering.

Dr. J. Ashley Taylor and Dr. Daniel Vitkavage, from Lucent Technologies, Bell Laboratories, in Orlando, FL, had an early influence on my interest in plasma etching and RIE. They took me in and taught me the details. Their approach to research and development in the filed of microfabrication was an excellent example which has served as a foundation for me to build upon.

It is an honor to associate myself with my advisor, Dr. Stephen Pearton. He is a world recognized expert in the field of RIE and a world-class mentor-professor. He has played a very important role in both my academic and professional development.

Dr. Robert Norwood and Dr. Robert Mininni from Photon-X have been strong proponents of this work. They have supported my ideas and have been extremely encouraging throughout this effort.

My wife Christine has been a pillar of strength and a source of encouragement throughout my many years of graduate school. Her patience and support has been a tremendous asset though these years and have made it possible for me to achieve my goals.

My parents are my foundation in all aspects of my life. They have inspired my goals and have given me all the means with which to pursue them.

TABLE OF CONTENTS

page

ACKNOWLEDGMENTS iv

LIST OF TABLES ix

LIST OF FIGURES xi

ABSTRACT xiv

1 INTRODUCTION AND MOTIVATION 1

2 LITERATURE REVIEW 6

- 2.1 Introduction 6
- 2.2 Polymer Optical Devices 6
  - 2.2.1 Background 6
  - 2.2.2 Polymer Optic Components 9
  - 2.2.3 Polymer Waveguide Technology 12
- 2.3 Polymer Optic Materials 15
  - 2.3.1 Hydrocarbon Polymer Materials and Thin Films 17
  - 2.3.2 Fluoropolymer Thin Films 19
- 2.4 Plasma/Reactive-ion Etching 22
  - 2.4.1 History 23
  - 2.4.2 Etching Fundamentals 23
  - 2.4.3 Polymer Etching 28
    - 2.4.3.1 Thermal process restriction 29
    - 2.4.3.2 Etch surface roughness evolution 30

3 EXPERIMENTAL METHODS 31

- 3.1 Introduction 31
- 3.2 Sample Processing 31
  - 3.2.1 Polymer Photonic Device Fabrication 32
  - 3.2.2 Experiment Sample Fabrication 33
    - 3.2.2.1 Surface activation using oxygen plasma 35
    - 3.2.2.2 RIE surface microfeature formation 35
- 3.3 Experimental Design 36
- 3.4 Analytical Surface Analysis 36
  - 3.4.1 Optical Microscopy 36
  - 3.4.2 Scanning Electron Microscopy 37

3.4.3 Atomic Force Microscopy 37
3.4.4 Stylus Profilometry 39
3.4.5 Contact Angle Measurement 39
3.4.6 X-Ray Photoelectron Spectroscopy 41
3.4.7 Fourier Transform Infrared Spectrometry (FTIR) with Horizontal Attenuated Total Reflectance (HATR) 42
3.5 Adhesion Testing 44
3.6 Environmental Performance Testing 46
3.6.1 Temperature Cycling Test 46
3.6.2 Accelerated Thermal Shock Testing 47
3.6.3 Damp Heat (85°C - 85%RH) Test 47
3.6.4 Accelerated Moisture/Temperature Testing 48

4 SURFACE ACTIVATION USING OXYGEN GAS PLASMA 49

4.1 Background 49
4.2 Results 53
4.2.1 Structural Characterization 55
4.2.1.1 Profilometry 55
4.2.1.2 Atomic force microscopy 57
4.2.1.3 Contact angle measurement 73
4.2.1.4 XPS 75
4.2.1.6 Fourier transform infrared spectrometry (FTIR) 79
4.2.2 Adhesion Characterization 80
4.3 Discussion 83
4.3.1 Structural Morphology 83
4.3.1.1 Surface structure alteration and measurements 83
4.3.1.2 Chemical modification 85
4.3.2 Adhesion Characterization 86
4.4 Summary 89

5 RIE SURFACE MICROFEATURE FORMATION 92

5.1 Background 92
5.2 Results 97
5.2.1 Structural Characterization 97
5.2.1.1 SEM analysis 97
5.2.1.2 Profilometry analysis and etch roughness evolution 99
5.2.1.3 XPS analysis 102
5.2.2 Adhesion Characterization 104
5.3 Discussion 104
5.3.1 Structural Characterization 104
5.3.3 Etch Roughness Evolution 105
5.4 Summary 106

6 ENVIRONMENTAL DEVICE TESTING 108

6.1 Background 109
6.2 Results 114
    6.2.1 Telecrodia Temperature Cycling Test 114
    6.2.2 Accelerated Temperature Cycling Test 117
    6.2.3 Damp Heat (85°C - 85%RH) Test 117
    6.2.4 Accelerated Damp Heat Test 120
    6.2.5 Post Environmental Test Adhesion Scratch Testing 120
6.3 Discussion 123
6.4 Summary 124

7 CONCLUSIONS 125

7.1 Blanket Oxygen Plasma Treatment 125
7.2 Etched Microstructure Feature Formation 126
7.3 Testing of Long Term Performance and Reliability 126
7.4 Future Work 127

A CROSS HATCH SCRATCH TEST BLADE SPECIFICATION 130

B BROADBAND CONTACT PHOTOLITHOGRAPHY 131

LIST OF REFERENCES 132

BIOGRAPHICAL SKETCH 136

LIST OF TABLES

Table page

1-1. Copper vs. fiber capacity comparison. 2

2-1. Vibrational bond structures and absorption losses at selected wavelengths of interest....20

3-1 Analytical data model for A-Bisphenol Polycarbonate XPS analysis....42

4-1. Surface energy values of common plastic materials 51

4-2. Untreated/plasma treated contact angle measurements for various polymers....52

4-3. Sample identification and plasma treatment conditions....54

4-4. AFM roughness measurement data summary. 66

4-5. Constant etch depth experiment matrix....68

4-6. AFM measurement data summary – constant etch depth roughness results....72

4-7. Post treatment contact angle measurements for experimental matrix conditions. 74

4-8. XPS peak distribution data analysis from fresh sample 77

4-9. XPS peak distribution data analysis from clear sample 77

4-10. XPS peak distribution data analysis from etched sample....78

4-11. Scratch test adhesion results for blanket oxygen treatment....80

5-1. Screening experiment matrix for microfeature evaluation. 96

5-2. Pattern size vs. etch roughness evolution....100

5-3. XPS peak distribution data for tight pitch patterned sample etched to 60µm 103

6-1. Telecordia GR-1312-CORE reliability test standard for gain block and amplifier module....109

6-2. Environmental testing experimental matrix. 113

6-3 Boiling/Freezing Water Immersion Test Results 117

6-4. Pressure cooker accelerated damp heat test results. 120

LIST OF FIGURES

Figure page

1-1. Attenuation of silica glass fiber. 3

2-1. Fiber optic communications system structure. 7

2-2. Optical waveguide technology 8

2-3. Polymer Waveguide Cross Section. 8

2-4. Fiber optic cable spectral performance....10

2-5. All-optical component ICs....11

2-6. Candidate polymer materials platform. 12

2-7. Polymer optic device fabrication process. 13

2-8. Optical materials spectrum 14

2-9. Polymer optical transmission spectrum. 15

2-10. Polytetrafluoroethylene (PTFE) transmission spectrum....16

2-11. Teflon AF chemical monomer structure....17

2-12. Near infrared absorption loss....18

2-13. Fluoropolymer structure and molecular bonding affinity....19

2-14(a-b) Molecular structure of fluoropolymer(a) vs. hydrocarbon Polymer(b) 21

2-15. The dry etching spectrum 25

2-16. Typical system configurations for etching 26

2-17(a-c). Dry etch mechanisms....27

3-1. Cross section of a polymer waveguide device....32

3-2. Reactive ion etching method for waveguide fabrication. 33

3-3. MxP+ etch chamber schematic 34

3-4. Digital instruments AFM equipment configuration schematic 38

3-5. Contact angle measurement 40

3-6. Contact angle analysis configuration 40

3-7. Typical XPS analysis configuration. 41

3-8. Molecular model for A-Bisphenol polycarbonate. 42

3-9. FTIR analysis equipment configuration 43

3-10. Horizontal attenuated total reflectance sampling method for FTIR. 44

3-11. Elcometer model 107 cross hatch cutter blades 45

3-12. Temperature cycling program profile. 47

4-1. Molecular structure of A-Bisphenol polycarbonate. 51

4-2. Surface roughness evolution during oxygen etching of polycarbonate. 55

4-3. Polycarbonate material removed vs. oxygen etch time. 56

4-4. AFM micrograph of virgin polycarbonate surface 58

4-5(a-d). AFM analysis at Constant Time/ Variable Pressure and Power 59

4-6(a-h). AFM analysis at Constant power and pressure 62

4-7. RMS roughness etch factor interaction profiles for variable etch time, power and pressure conditions 67

4-8. Surface area etch factor interaction plots for variable etch time, power and pressure conditions. 68

4-9(a-e). AFM micrographs for constant etch depth variable pressure and power. 69

4-10. RMS roughness etch factor interaction profiles for constant etch depth conditions. 72

4-11. Untreated polycarbonate substrate sessile drop test. 73

4-12. Oxygen treated polycarbonate substrate sessile drop test. 74

4-13. Main effect analysis for contact angle measurements 75

4-14(a-c). XPS analysis raw count data for bulk, masked, and etched areas. 76

4-15. FTIR spectrum analysis of etched and unetched polycarbonate surface.................79

4-16. Factor midpoint scratch test results main effects analysis......................................81

4-17. Scratch test results main effects analysis – gentle plasma conditions.....................81

4-18. Scratch test results main effects analysis – aggressive conditions...........................82

4-19. Scratch test results main effects analysis – optimal conditions...............................82

4-20. Multivariate scatterplot of adhesion test analytical result relationships..................88

5-1(a,b). Microfeature covered substrate surface(a) and cross section profile(b). 94

5-2. Mask pattern for microfeature evaluation experiment – optical micrograph. 95

5-3(a-d). SEM micrographs of etched microstructures; (a) 5μm x 5μm x 7μm (length x width x height), (b) 10μm x 10μm x 7μm, (c) 5μm x 5μm x 15μm, (d) 10μm x 10μm x 15μm...98

5-4. Mask pattern Size vs. etch roughness..101

5-5. Average peak – valley measurement..102

5-6. XPS analysis raw count data for tight pitch patterned sample etched.....................103

6-1. Water vapor attack on film-substrate interface...110

6-2. Network thin film cracking due to stress effects. 111

6-3. Optical micrograph showing an example of thin film de-lamination from the substrate. 112

6-5(a-f). Pre/post (1000hrs) damp heat test results...118

6-6. Optical micrograph of cross hatch scratch test on fully fabricated device with no substrate surface treatment...121

6-7. Optical micrograph of cross hatch scratch test on fully fabricated device with no substrate surface treatment...122

6-8. Optical micrograph of cross hatch scratch test on fully fabricated device with no substrate surface treatment...123

Abstract of Dissertation Presented to the Graduate School
of the University of Florida in Partial Fulfillment of the
Requirements for the Degree of Doctor of Philosophy

PLASMA ETCHING FOR ADVANCED POLYMER OPTICAL DEVICES

By

Donald Stephen Bitting

December 2003

Chair: Stephen Pearton
Major Department: Materials Science and Engineering

Plasma etching is a common microfabrication technique which can be applied to polymers as well as glasses, metals, and semiconductors. The fabrication of low loss and reliable polymer optical devices commonly makes use of advanced microfabrication processing techniques similar in nature to those utilized in standard semiconductor fabrication technology. Among these techniques, plasma/reactive ion etching is commonly used in the formation of waveguiding core structures. Plasma etching is a powerful processing technique with many potential applications in the emerging field of polymer optical device fabrication. One such promising application explored in this study is in the area of thin film-substrate adhesion enhancement.

Two approaches involving plasma processing were evaluated to improve substrate-thin film adhesion in the production of polymer waveguide optical devices. Plasma treatment of polymer substrates such as polycarbonate has been studied to promote the adhesion of fluoropolymer thin film coatings for waveguide device fabrication. The effects of blanket oxygen plasma etchback on substrate, microstructural substrate feature formation, and the long term performance and reliability of these methods were investigated.

Use of a blanket oxygen plasma to alter the polycarbonate surface prior to fluoropolymer casting was found to have positive but limited capability to improve the adhesive strength between these polymers. Experiments show a strong correlation between surface roughness and adhesion strength.

The formation of small scale surface features using microlithography and plasma etching on the polycarbonate surface proved to provide outstanding adhesion strength when compared to any other known treatment methods.

Long term environmental performance testing of these surface treatment methods provided validating data. Test results showed these process approaches to be effective solutions to the problem of adhesion between hydrocarbon based polymer substrates and fluoropolymer thin films.

CHAPTER 1
INTRODUCTION AND MOTIVATION

The first optical communication system was invented in 1880 with the invention of the photophone by Alexander Graham Bell [1]. Not until 1960 with the invention of the laser, and 1970 with the development of the first truly low-loss fiber did the field of optical communications begin to take form. Over the past 25 years society has experienced a global revolution in communications technology. This revolution had its genesis in the form of a fully electronic infrastructure. Advances in hardware technology (silicon) and software applications throughout the 1980s and 1990s presented many new data and voice products/applications reaching many more consumers than ever before. This tremendous growth in the communications industry has created a demand for further advancements in high speed/high bandwidth communications. Communication system provider companies have struggled to keep up with customer demand for more information through the growth of telephone systems, the Internet, expansion of cable television programming, and more widespread deployment of local area computer networks. These companies are approaching limitations in their ability to meet customer demands. This is primarily due to the limitations of their hardware technology which most often relies on an electronic or optoelectronic component infrastructure. Computer networks as well as telephone systems were born out of networks that were able to interact with each other via copper cables and components carrying/processing electrical signals.

The next progressive step to providing customers with higher speed communication access is to migrate to an all-optical device/system infrastructure. These systems utilize photons instead of electrons to carry, route, and process data across their networks. All-optical networks are faster than conventional ones. They also provide significantly greater bandwidth as shown by the comparison in Table 1-1 and can carry signals for much greater distances without need for signal amplification. Optical systems have been hailed as the cure for the next generation of communication networking. We presently find ourselves in this second (optical networking) phase of this communications revolution. These systems are built upon dense wavelength division multiplexing (DWDM) technology, which is a powerful capability of optical fiber and signal processing systems.

Table 1-1. Copper vs. fiber capacity comparison [2,3].

	Distance	Bandwidth/Speed	# Data Channels
Twisted Copper Pair	2.5 Km	300 BPS – 10 MBPS	24
Coaxial	2.5 Km	56KBPS – 200 MBPS	
Optical Fiber	200 Km	500 KBPS – 6.4 TBPS	32,000+

Note: BPS = bits per second; K = Kilo; M = Mega; G = Giga; T = Tera.

When fiber optic lines are used in a system, the focus turns to the component level as the limiting factor in performance. Components such as amplifiers, multiplexers, and switches are required in any system to route and process signals. Electronic based components within a fiber backbone network require conversion techniques to change the optical signal to an electronic one for processing and then back again. These frequent conversions can significantly slow down the speed of a network. This is the primary motivation for all optical components which do not require signal conversion. The development of all optical components is the primary focus in the advancement of this new generation of communications.

Most present-day all-optical communication hardware components and fibers are made from silica. Silica glass is an attractive material for optical communication due to very low intrinsic absorption loss characteristics in the near-infrared optical spectrum as shown in Figure 1-1, and the ability to draw long length fibers.

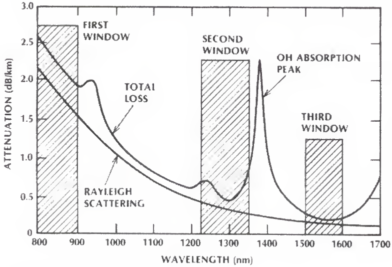

Figure 1-1. Attenuation of silica glass fiber [4].

An alternate recognized approach to making these fibers and components involves the substitution of glass with polymer materials to guide and route the optical signals. Plastic optical fibers have been demonstrated but still have many processing/performance issues. Plastic fibers are not yet practical as their attenuation performance is far inferior to that of silica glass fibers.

Although not attractive as a fiber alternative, polymers are well suited for use at the component level. Specialized polymers exist which present significant potential advantages over glass in terms of performance and integration when short distances (<500cm) are considered. This makes the development of a polymer system for waveguide processing of prime interest for use with silica based fiber networks.

One of the difficulties in fabricating polymer devices lies in the requirement to use specialized perfluorinated polymer (fluoropolymer) materials as they have proven superior when their performance is compared to that of common hydrocarbon optical grade polymers such as polycarbonate or poly-methyl methacrylate (PMMA). The use of fluoropolymers in these devices presents a unique challenge as they are inherently difficult to process and do not adhere well to many other materials. In addition, fluoropolymers are significantly more expensive than hydrocarbon polymers and thus must be used sparingly in the overall design of the device.

The ever expanding demand for high speed communications and bandwidth will continue to push demand for cost effective and reliable all-optical devices. This work is devoted to finding an engineering solution to one of the primary problems encountered when attempting to fabricate polymer waveguide devices for all-optical communications in the adhesion of fluoropolymer thin films to hydrocarbon polymer substrates. To investigate this phenomenon and to find an engineering solution, the effect of both chemical and mechanical surface treatments using plasma etching and RIE were evaluated.

A review of the literature is presented in Chapter 2. This provides relevant background information related to the properties of fluoropolymers and hydrocarbon polymers, plasma and reactive ion etching and their application to polymers, and information on adhesion testing of polymer materials. The experimental method is discussed in Chapter 3 showing the techniques, conditions, and characterizations used to evaluate the process effectiveness of the surface treatments evaluated. Results and discussion around experimental designs used to evaluate the effect of a blanket oxygen plasma etchback approach are presented in Chapter 4. Chapter 5 contains the results and discussion of the designed experimentation to evaluate the effectiveness of microstructural feature formation through patterning and plasma etching/RIE. The study in Chapter 6 was designed to test and evaluate these surface modification techniques evaluated in Chapters 4 and 5 under wide ranging environmental test conditions to assess the reliability of devices fabricated using these methods. Chapter 7 is a discussion of the overall conclusions that can be drawn from this work as well as future work to be performed.

Finally, it is worth noting that although this work was motivated by the industry demand to develop fluoropolymer based all-optical communications devices, there are many other applications which could benefit from these findings. Additional areas of potential application include microfluidic medical/pharmaceutical devices, organic integrated circuits, and PEM fuel cells. Beyond all plastic devices, there are various new end applications where plastic substrates are being investigated. A recent article in *Forbes* magazine highlighted the effort currently being undertaken at the DuPont company in a joint venture with Sarnoff focused on "looking for a way to print electronics on to plastic instead of the more expensive silicon" [5]. This work will be insightful and applicable for a broad range of materials used in conjunction with plastic substrates.

CHAPTER 2
LITERATURE REVIEW

2.1 Introduction

This work is focused on understanding the role of plasma/reactive ion etching in promoting adhesion between fluoropolymer thin films and hydrocarbon polymer substrates to enable cost effective and reliable polymer optic devices. This chapter reviews the background information related to polymer optical devices, the bonding/adhesion fundamentals of fluoropolymer materials, and the fundamental aspects of plasma/reactive ion etch processing. The section covering polymer optic devices provides a broad overview of polymers and their use in the field of optical communications. The polymer optic materials section gives specific attention to polycarbonate and fluoropolymer materials and how their material properties affect adhesion to other materials and surfaces. An overview of plasma/reactive ion process fabrication is presented with particular attention given to the use of this technique when applied to polymer materials.

2.2 Polymer Optical Devices

2.2.1 Background

Communications have conventionally been electronic in nature. Recent advances have shown the benefits of moving from electronic to optical systems to carry and route information signals. This will expand the capacity and improve the speed of information networks. An example of a typical fiber optic communication system is shown in Figure 2-1.

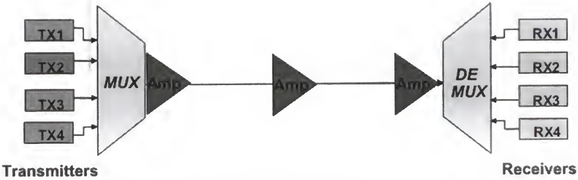

Figure 2-1. Fiber optic communications system structure.

Multiple channels are combined (multiplexed) and sent over a single fiber optic cable to their final destination where the signals are separated (de-multiplexed) and individually re-routed. Amplifier devices are required to periodically boost the signal strength which experiences loss during travel. There are many different types of optical devices required in the operation of a fiber optic communications system such as switches, multiplexers, de-multiplexers, and amplifiers to name only a few.

All optical components offer significant advantages in bandwidth. These devices can be categorized as free space, fiber based, or integrated (waveguide based). Integrated optical devices are critical in the evolution process from electronic systems to optical systems due in part to their compact size. The size of integrated optical components can be similar in dimension to their electronic counterparts. This is an important product aspect as space limitations are a significant consideration in the communications industry. Integrated optical components typically comprise those devices implementing waveguide-based technology as opposed to free space or fiber based technology. An example is shown in Figure 2-2. A slab (2-dimensional) waveguide is shown here with requirements that n_s and n_c both be lower than the index of the waveguide for total internal reflection.

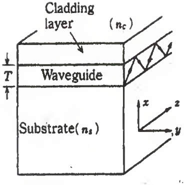

Figure 2-2. Optical waveguide technology [6].

Waveguide devices have traditionally been fabricated using silica material for its very low loss characteristics and capability within the system to perform index tuning. In addition, silica technology is a well-established technology in microelectronic device fabrication. Polymer waveguides have been gaining interest in the field of optical device technology due to their relatively low cost and unique affinity for large-scale integration. Polymer waveguide photonic ICs have been demonstrated in both hydrocarbon polymer and fluoropolymer materials. These plastic ICs present a novel materials platform with significant performance and cost potential over conventional platforms such as silica. A cross section of a 3-dimensional polymer waveguide device showing a rib waveguide on a substrate is shown in Figure 2-3.

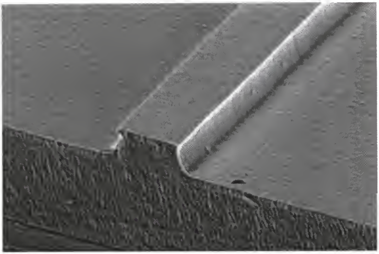

Figure 2-3. Polymer Waveguide Cross Section.

Polymer waveguide technology is a relatively unproven platform in the optical devices industry. This is primarily due to serious concerns about the long term reliability of polymer materials. Many people feel more comfortable with silicon/silica technology. Silica has been used for many years in the semiconductor industry and there is a lot of existing literature. There are many processing challenges which must be overcome to make low loss and reliable polymer waveguide device fabrication possible. Unlike silica, polymer materials have unique inherent material properties which place restrictions on processing methodologies and conditions. In the case of fluoropolymers, for example, thin film adhesion issues are a significant concern. Many polymers possess a relatively low glass transition temperature which presents thermal processing restrictions. The ability to perform index tuning in polymers is more difficult than in an inorganic system such as silica.

2.2.2 Polymer Optic Components

Components for optical communications have traditionally relied on the silicon/silica platform. This technology is widely accepted and has been successful in enabling many advanced systems and components. As mentioned previously, this platform is a well established system from many years of development for semiconductor devices. An additional reason for acceptance lies in the likeness of the platform to fiber optic cables. Silica is a natural platform as the installed base of optical communications systems consists of silica fiber optic cable with spectral performance as shown in Figure 2-4 which shows the spectral range of wavelengths between 1200 and 1700nm. The ability to utilize components made from material as close as possible to that of the fiber provided a level of comfort to engineers and customers.

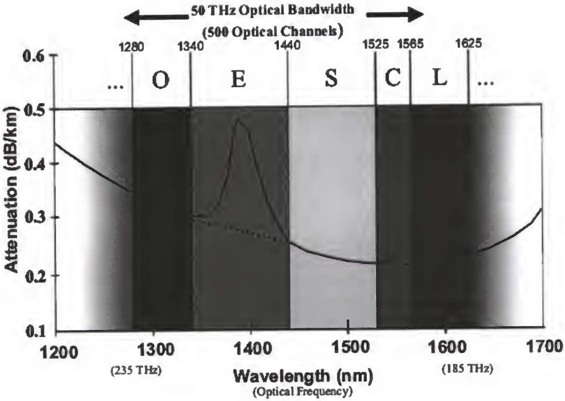

Figure 2-4. Fiber optic cable spectral performance.

Glass based optical fiber exhibits excellent optimal performance in the O, S, C, and L bands. The E band is plagued by a large loss attenuation peak. It is well known that this attenuation peak is due to water absorption in the silica. The source of this water in the silica has its origin in the fabrication process of producing glass fibers from preforms. Although low loss communication is possible in various bands, the C band (around 1550nm) is used most widely due to the availability of rare earth dopants such as erbium, for example, which enable signal amplification via 980nm pumping and stimulated emission. Recent work has been performed which also shows promise for amplification capability in the O band (around 1310nm) using chromium embedded nanoparticles. For these reasons, any optical communication device must be capable of low loss light guiding at both 1550nm and 1310nm wavelengths. For these reasons, planar silica technology has been the industry standard platform with loss performance very closely mirroring that of fiber optic cable.

It has been known for a long time that optical grade polymers are theoretically capable of performing on par with and potentially outperforming silicon/glass based systems. Polymers, for example, have been used widely in the field of optometry for many years.

Polymers traditionally accepted as having optical grade properties include PMMA, polycarbonate, and the fluoropolymers. This designation derives from their ability to guide light with low signal loss due to intrinsic absorption effects.

The various components that can be fabricated in the silicon/silica materials system can also be fabricated using polymers. The most common of these all-optical components are shown in Figure 2-5.

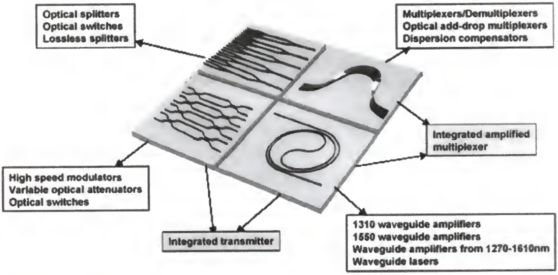
Optical splitters
Optical switches
Lossless splitters
Multiplexers/Demultiplexers
Optical add-drop multiplexers
Dispersion compensators
Integrated amplified multiplexer
High speed modulators
Variable optical attenuators
Optical switches
Integrated transmitter
1310 waveguide amplifiers
1550 waveguide amplifiers
Waveguide amplifiers from 1270-1610nm
Waveguide lasers

Figure 2-5. All-optical component ICs.

Passive devices such as multiplexers and splitters have already been successfully demonstrated in a polymer system. Active devices such as thermo-optic modulators and optical signal amplifiers are presently in development. The development of low loss and reliable devices and components which are capable of performance level similar or better than silica is a key factor in moving polymer components from development and demonstration to mainstream acceptance and implementation.

2.2.3 Polymer Waveguide Technology

An example of a typical 3-dimensional polymer based waveguide platform is presented in cross section in Figure 2-6. In such a system, low loss polymer thin films with slightly different index of refraction values (typically less than 1% apart for single mode operation) are used to compose the core and cladding. The substrate is composed of an inexpensive polymer such as polycarbonate as opposed to a semiconductor material. The polymer substrate is used simply as a mechanical medium upon which to perform thin film fabrication processing. Since the substrate does not act as an optical medium, the mechanical material compatibility is the primary consideration. One of the

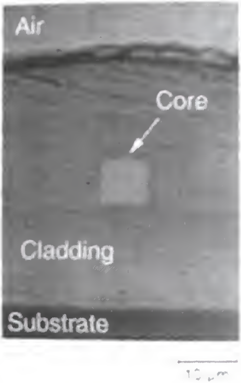

Figure 2-6. Candidate polymer materials platform.

most significant attributes of a polymer-based substrate over that of a semiconductor is the capability to perform CTE (coefficient of thermal expansion) value matching [7]. Polymer thin film processing commonly requires many thermal processing steps which typically are in approach of the T_g of the polymers. Mismatch of CTE can lead to product performance issues such as cracking and stress induced loss.

Low loss polymer devices are fabricated in a cleanroom environment using spin casting of polymer solutions and thin film curing along with microfabrication techniques such as photolithography, chemical processing, and dry etching. Figure 2-7 represents the standard process flow for polymer device fabrication.

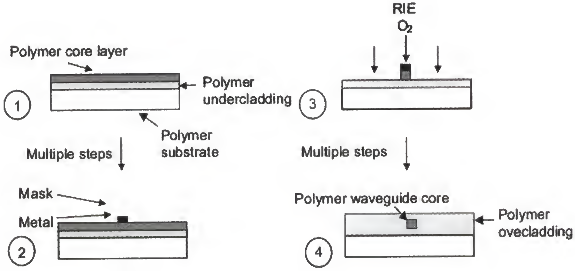

Figure 2-7. Polymer optic device fabrication process.

The fluoropolymer core/clad with polycarbonate substrate material platform is a promising candidate for use in the fabrication of polymer optical components. This advanced platform is the focus of the following work. Theoretical simulations show that this platform is capable of superior performance when compared to the silicon/silica platform or those based wholly on hydrocarbon polymers.

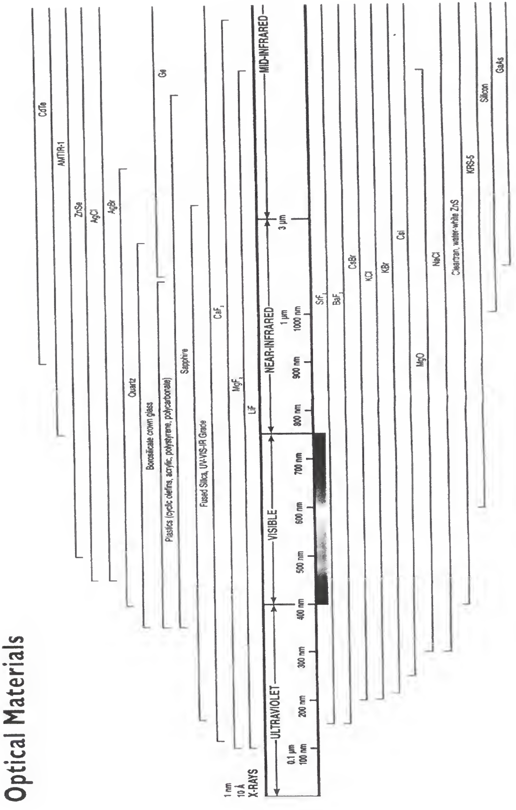

Figure 2-8. Optical materials spectrum [8].

2.3 Polymer Optic Materials

Polymers are among a limited group of materials considered to exhibit exceptional optical properties in both the visible and near infrared spectral ranges as shown by Figure 2-8. Their high transmission characteristic in the near-infrared spectrum make polymers a viable class of material for optical communication. As a substitution for glass, they are one of the most attractive candidates due to their great abundance, durability, and low cost.

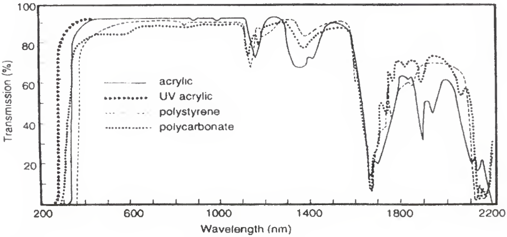

Figure 2-9. Polymer optical transmission spectrum.

Figure 2-9 shows optical transmission spectra for a number polymers frequently used for optical communications. Many optical plastics transmit well in the visible and the near infrared, but absorb strongly in the ultraviolet and the mid-far infrared. Most plastics degrade somewhat both in physical and optical properties when exposed to ultraviolet radiation [9].

Fluoropolymers are a class of polymers which possess particularly outstanding optical clarity in both the visible and near infrared range as shown in Figure 2-10.

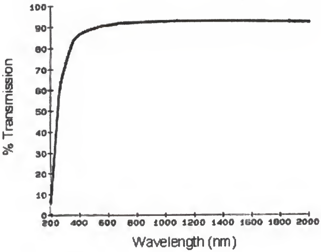

Figure 2-10. Polytetrafluoroethylene (PTFE) transmission spectrum.

Perfluorinated polymers are considered to be the most promising of the optical grade polymer materials due to their exceptional high degree of optical clarity in the near infrared region.

The optical transparency of perfluorinated polymers is partly derived from the fundamental characteristics of C-F bonding which is much less susceptible to light absorption losses due to vibrational motions than that experienced by the C-H bond [10]. Higher degrees of fluorination replace C-H bonds which results in less loss from absorption. The most effective polymers possess a high level of flourination. The near infrared optical performance of these materials make them extremely attractive candidates for use in optical communication devices. The degree of crystallization is another property of polymers/fluoropolymers which can adversely affect their performance. Crystalline regions in the polymer will have a negative affect on loss. Optical differences between crystalline and non-crystalline domains can lead to optical scattering effects. Highly amorphous polymers/fluoropolymer structures such as Teflon® AF (DuPont 1989) are preferred for use in optical devices. Teflon® AF is a copolymer of the structure

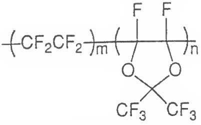

Figure 2-11. Teflon AF chemical monomer structure.

shown in Figure 2-11. The physical structure of the copolymer prevents the formation of crystalline regions within the microstructure. The prevention of crystalline regions is critical in the pursuit of low loss waveguides.

Polymer optic materials comprise a small set of select hydrocarbon, partially fluorinated, and perfluorinated polymers which exhibit relatively low absorption loss characteristics. An understanding of the basic materials properties of hydrocarbon polymer and fluoropolymers is presented. Partially fluorinated polymer materials are simply a mix between these two cases. An understanding of these fundamental materials properties is critical for the design, processing, and testing of optical devices and components.

2.3.1 Hydrocarbon Polymer Materials and Thin Films

Conventional polymer optical components were investigated in the early 1980s by optical component pioneering companies such as AT&T and NTT. The first components were manufactured using hydrocarbon-based polymers such are PMMA, Polyimide, and polycarbonate materials. Of these, PMMA has been used most extensively with the lowest loss results for planar optical devices.

Successful waveguide based devices have been built using these materials. Significant literature has been published on structures/devices built using PMMA.

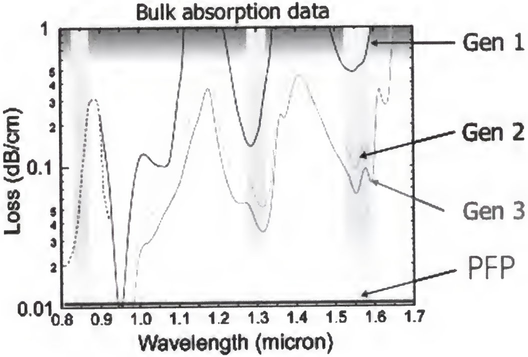

Figure 2-12. Near infrared absorption loss.

These polymers were among the first to be evaluated for optical devices due to their relatively low loss optical performance in the near infrared optical spectrum when compared to other common polymers. Devices fabricated with these polymers produced 1550nm wavelength bulk intrinsic absorption results on the order of .1 - .7 db/cm as represented by results GEN1, GEN2, and GEN3 in Figure 2-12.

The generational progression is representative of the various stages of material development in the field of polymer optical devices. Generation 1 polymers were primarily based on PMMA (poly-methyl methacrylate). Generation 2 consisted of polyamide-imides (PAI). In generation 3, partial fluorination of PMMA/PAI was introduced. Perfluorinated polymers (represented by PFP on the graph in

Figure 2-12) present a new realm of possibility as they can exhibit extraordinarily low absorption loss.

2.3.2 Fluoropolymer Thin Films

Perfluorinated polymers such as PTFE, shown in Figure 2-13, have many properties which make them unique when compared to hydrocarbons.

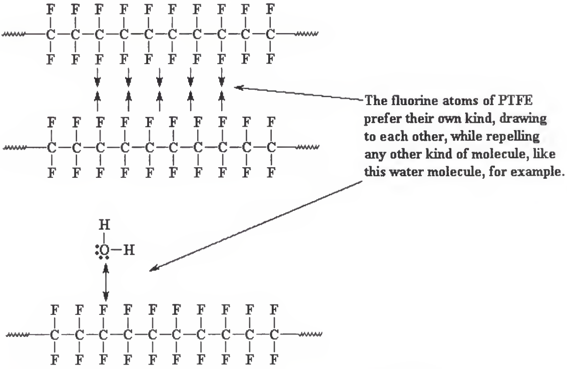
F
C
H
O
The fluorine atoms of PTFE prefer their own kind, drawing to each other, while repelling any other kind of molecule, like this water molecule, for example.

Figure 2-13. Fluoropolymer structure and molecular bonding affinity [11].

They are most commonly described as hydrophobic with enhanced thermal, chemical, and oxidative stability; reduced adhesion; improved biocompatibility; and increased gas permeability. The fundamental root causes of these factors lies in the electronegativity difference between the two which is derived from a higher bond strength of C-F bonds in comparison to that of C-H [12].

These polymers are considered to be the most appealing candidates for use as an optical transmission medium due to the low absorption loss for optical signals.

Fluoropolymers exhibit insignificant signal loss when compared to hydrocarbon polymers which are plagued by adsorption losses created by the C-H bond. The fundamental reason for this loss lies in the absorption peaks due to anharmonic vibrational oscillation modes given and their relative locations in the infrared spectral region. Table 2-1 shows selected bond structures and the intensities of vibrational modes within the infrared region of interest.

Table 2-1. Vibrational bond structures and absorption losses at selected wavelengths of interest [13].

Bond	Wavelength (nm)	Intensity (a.u.)	Absorption (dB/cm)
C-H	n1 = 3390	1	500
C-H	n2 = 1729	7.2×10^{-2}	36
C-H	n3 = 1176	6.8×10^{-3}	3.4
C-F	n5 = 1626	6.4×10^{-6}	.0032
C-F	n6 = 1361	1.9×10^{-7}	.000095
C-F	n7 = 1171	6.4×10^{-9}	.0000032
C-O	n3 = 1836	1.2×10^{-2}	6
C-O	n4 = 1382	4.3×10^{-4}	.22
C-O	n5 = 1113	1.8×10^{-5}	.009

The C-H bond has a first order harmonic mode at 3390nm with strong second and third overtone modes extending in to the near infrared (1300-1700 nm) region. In the case of the C-F bond, the near infrared region in not affected until the fifth, sixth, and seventh overtone modes are considered. These higher order modes are extremely weak and do not result in significant absorption loss [14].

Although fluoropolymers are superior in performance, they have limitations which must be overcome prior to successful implementation in to optical components. They are notoriously difficult to process due to their low surface energy and their materials properties which are derived from their atomic bond characteristics and orientations as in Figure 2-14(b). These properties pose significant limitations on their manufacturability when compared to hydrocarbon based materials such as that in Figure 2-14(a) which exhibit less shielding of the carbon backbone.

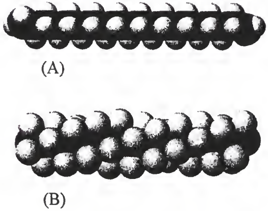

Figure 2-14(a-b) Molecular structure of fluoropolymer(a) vs. hydrocarbon Polymer(b) [15].

Fluoropolymers have low surface energy and mechanical strength compared to hydrocarbon polymers. This property results in poor adhesion with other materials. One example of this is evident in the application of non-stick cookware where fluoropolymer coatings are applied to a metal surface. This non-stick property is a great advantage when the interaction between the cooking food and the polymer surface is considered. The same properties prevent the fluoropolymer materials from naturally adhering to the metal. Elaborate methods for enhancing adhesion to the metal surface are required as disclosed by Deng and Tsai [16]. Unconventional approaches to fluoropolymer processing have been employed to accommodate their unique properties which are many times the same properties which make fluoropolymers attractive in the end product application.

Fluoropolymer usage in the design of overall components must be limited due to their relatively high cost. Typical costs range from \$12-\$18 per pound. This is a drastic premium when compared to other commercial hydrocarbon polymers which typically run between \$0.40 and \$2.70 per pound. The high cost of fluoropolymers is a limiting factor in their utilization.

These polymers exhibit superior clarity when compared to other polymers over a very wide spectrum. Bulk absorption loss in the near infrared region is much better than that of hydrocarbon based polymers by an order of magnitude. PTFE can be crystalline in nature which is not desirable for waveguide devices. New perfluorinated polymer materials such as Teflon® AF have been developed which are amorphous in nature for use in waveguide fabrication. Figure 2-12 shows bulk absorption loss for amorphous perfluorinated polymers (PFP) around .01db/cm. This theoretical performance level (if achieved) could place polymer waveguides ahead of silica waveguide technology which presently performs on the order of .03db/cm.

2.4 Plasma/Reactive-ion Etching

This work focuses on the utilization of plasma etching as a means for improving materials system performance. Plasma etching is a common microfabrication technique. An understanding of this scientific discipline is necessary to comprehend the experiments carried out for this work. This section provides an overview of the background and fundamental of plasma etch processing. Since plasma etching is most commonly used for the processing of inorganic materials and thin films, the final sections are devoted to the science of polymer etching as well as consideration of various plasma processing issues unique to these materials.

2.4.1 History

Plasma processing in the production of semiconductor devices has been around since the early 1970s. Prior to this, wet chemical etching methods had been used to transfer patterned features to wafers. Reactive ion etching (RIE) was discovered in the mid-late 1970s by implementing electrostatic sheaths in to the chamber to enable ion acceleration from the plasma incident to the wafer surface. The combination of physical ion bombardment with chemically reactive species provided a synergistic method to produce vertically straight sidewalls. RIE quickly became a key factor in the ability to shrink minimum feature sizes from 6μm in 1976 to present day devices with minimum features on the order of .1μm [17].

2.4.2 Etching Fundamentals

The ultimate goal of an etch process is to selectively and physically transfer device features from a top masking layer to an underlying material. Pattern transfer using plasma etching occurs in the following manner: First, a film is deposited. This film is most commonly a semiconductor, dielectric, metal, organic polymer, or other materials depending on the type and function of the device being processed. Through a process known as photolithography, a pattern of polymeric photoresist is made as a mask to cover the etch candidate film or material. This photoresist is generally made to be somewhat etch resistant through a post expose bake process. This baking hardens the resist. Following post bake hardening, the resist can be used as an etch mask. The photoresist pattern is transferred to the underlying film or material by plasma etching which selectively attacks those areas of the etch target film or material not protected by the photoresist mask. Following this, the photoresist is selectively removed. The result is the inverse pattern of the photoresist etched in the underlying film.

Ion-assisted etching, also commonly referred to as dry etching or plasma etching, has the advantage of anisotropy which is typically unattainable by more conventional wet chemical etching methods.

Plasma etching is carried out within a chamber under partial vacuum. Depending on the particular system and the etch characteristics sought, the pressures used can range from .001 to 10 torr. The substrate is positioned in a stationary position and subjected to a plasma discharge created normal to the wafer surface (in the case of downstream sources, the plasma may be remote to the substrate surface). The many species created in the plasma are manipulated to interact with the substrate in a way that promotes the removal of the exposed material surface.

Plasma is a 4th state of matter and is a net neutral collection of positive and negative charged particles. Within this plasma exists (1) electrons, positive ions, negative ions; (2) neutral atoms, neutral molecules, radicals; and (3) photons emitted from de-exciting species [18]. In plasma etching, the plasma produces both highly reactive neutrals (e.g., atomic oxygen) and ions that bombard the surface being etched. The neutrals react with the surface to produce volatile species that desorb and are pumped away. Ion bombardment often increases the etching rate by removing surface contaminants that block the etching or by directly enhancing the kinetics of etching. The photons of various wavelengths which result from the excitation/de-excitation of the plasma species can be captured, analyzed by a spectrometer and the data fed back to the system to provide an endpoint signaling capability. System endpoint can be used to improve productivity by compensating for prior process nonuniformities.

As shown in Figure 2-15, there are a variety of dry etch process regimes. This figure indicates that the mechanism of etching for a given process can have a physical basis, a chemical basis, or a combination of the two (generally referred to as RIE which stands for reactive ion etching. As shown in the figure, pressure is the controlling factor for the etch mechanism. Lower pressures will produce more highly excited ions resulting from the higher mean free paths of the ions.

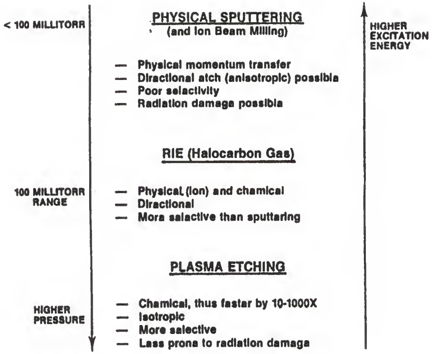
< 100 MILLITORR
PHYSICAL SPUTTERING
(and Ion Beam Milling)
HIGHER EXCITATION ENERGY
— Physical momentum transfer
— Directional etch (anisotropic) possible
— Poor selectivity
— Radiation damage possible
RIE (Halocarbon Gas)
100 MILLITORR RANGE
— Physical (ion) and chemical
— Directional
— More selective than sputtering
PLASMA ETCHING
HIGHER PRESSURE
— Chemical, thus faster by 10-1000X
— Isotropic
— More selective
— Less prone to radiation damage

Figure 2-15. The dry etching spectrum [19].

Figure 2-16 shows some examples of typical etching chamber configurations. 2-16(b) is representative of a capacitively coupled type reactor capable of producing plasmas of the concentration 10^8 ions/cm^3.

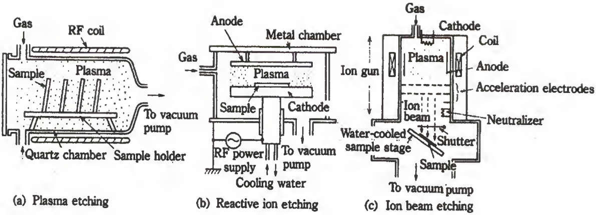

(a) Plasma etching (b) Reactive ion etching (c) Ion beam etching

Figure 2-16. Typical system configurations for etching [20].

For dry etching to occur, either the radical has to have a sufficient amount of heat kinetic energy or an ion has to possess a high amount of kinetic energy. If either situation is achieved, etching will proceed.

For the plasma etch case, shown in Figure 2-17(a), the progression of etching is dominated by radicals. The motion of these radicals has no set direction and so the etching will proceed isotropically. This etch will lead to significant undercut of the mask layer. It is not for use in applications where tight linewidth control is of critical importance.

The sputter etch case is shown in Figure 2-17(b). The progression of etching is dominated by ions. This figure shows the physical sputtering of a layer.

The RIE etch case is shown in Figure 2-17(c). Reactive ion etching, sometimes called reactive sputter etching, refers to a plasma etching process in which the plasma reactor is configured so that the ions attain high bombardment energies and significantly induce etching. Typically, this process is performed at low pressures where the ions passing through the plasma sheath suffer few collisions that would reduce the average ion bombardment energy.

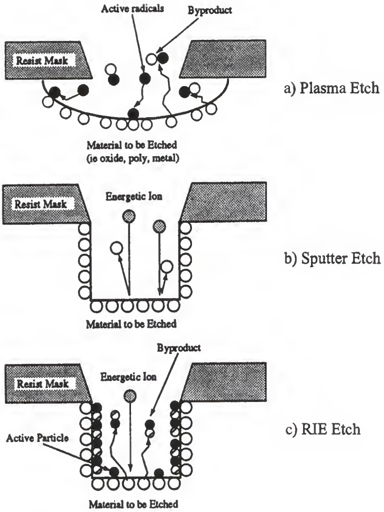

Figure 2-17(a-c) Dry etch mechanisms [21].

Dry etching requires a constant flow of feed gas. The feed gas/gasses used are highly dependent on the material to be etched except in the case of sputter etching which is a purely physical mechanism which does not rely on the chemical nature of the plasma species.

Etching is a complex but powerful process for use in advanced processing of materials. The primary factors in the development of an effective process include the feed gas/gas mixture selection, power level, pressure level, and chamber type/configuration.

2.4.3 Polymer Etching

The etching of polymer films and materials has not been widely studied. Until very recently, with the implementation of low-k dielectrics, polymer materials have not been commonly utilized in VLSI CMOS devices or related architectures. This is also true for integrated waveguide based photonic devices which have traditionally relied almost exclusively on silicon/glass based platforms. These are the primary industries which utilize plasma etching processes and equipment. Therefore, minimal data exists on the etching of polymer materials and the fundamental etch mechanism is not widely understood.

Oxygen based plasmas have been found to be quite effective for organic material dry etching. One of the more widely studied applications of polymer etching is in the process of photoresist removal or ashing. Zant proposes that the etching of simple photoresists commonly occurs according to equation 2-1 [22].

$$C_xH_y \text{ (resist)} + O_2 \text{ (plasma energized)} \rightarrow CO \text{ (gas)} + CO_2 \text{ (gas)} + H_2O \qquad (2\text{-}1)$$

Oxygen plasmas also naturally work very well when used to etch more complex polymers. Ko et al. suggests the primary etch mechanism for some hydrocarbon based polymers is believed to occur in two steps. In the first step, oxygen atoms attack and carry away the easily accessible hydrogen atoms from the polymer chain which leaves a radical species. Radicals react with oxygen to form carbonyl and alcohol groups which desorb from the surface and get carried away through the pumping system [23]. Fluorine gasses such as CF_4 have also been used for etching/surface modification of polymers as well as Argon [24,25].

Until recently, polymers have not been widely used materials for integrated electronic and photonic devices. Despite their many known advantages such as low cost and superior performance, there are a number of etch-related processing issues which have prevented them from widespread usage.

2.4.3.1 Thermal process restriction

One of the challenges with polymers processing is their low temperature tolerance. Most polymers have glass transition temperatures (T_g) between 100°C and 200°C. Plasma processing can produce significant heating from the plasma species interacting with the substrate surface. To prevent warping or melting of the polymers, process temperatures must be limited and/or the substrate must be cooled. This places restrictions on the range of processing parameters available. In general, high powers and low pressures generate more intense plasmas with higher energy characteristics. These factors must be limited to allow the polymer materials to dissipate heat. We know that polymers are generally not highly thermally conductive. Heat energy transferred to the polymers from the plasma environment is not readily dissipated. In addition to limitations on process factors, pulsed processing can be used to provide an opportunity for heat dissipation. Pulsed processing works by writing a program which etches (power on) for n seconds followed by a cooling step with no power for n seconds. During the cooling step, the substrate is convection cooled using a steady stream of helium. This cycle is repeated until the desired etch depth is reached. Even though the helium cooling is always on, the power off step provides an opportunity to reduce accumulated thermal energy. Helium cooling is conventionally applied to the back side of the substrate. Effective thermal management during an etching process presents limitations in process power and pressure which can have a significant impact on the etch sidewall profile. Complex programs can help to maintain thermal control of the material, but this approach is time consuming. For many devices where high temperature annealing is required for dopant distribution or implant annealing such as MOSFET transistors, polymers simply can not be used. For other devices, the ability to control thermal excursion is key to enabling the implementation of polymer technology.

2.4.3.2 Etch surface roughness evolution

Unlike many inorganic materials which result in smooth post etch surfaces, polymers have shown to exhibit surface roughness in post etch processed surfaces. This roughness is undesirable for many applications in which subsequent thin film processing is performed such as in waveguide structures where surface roughness can lead to poor device performance via scattering losses. In devices where extremely tight film tolerances are required, the roughness creates film dimension effects which are not acceptable. The understanding of etch roughness during etching and the factors which can be used to control this phenomenon is important in the implementation of polymer systems in to advanced devices. The ability to control this effect is important to enable polymer thin film surface property customization.

CHAPTER 3
EXPERIMENTAL METHODS

3.1 Introduction

This chapter discusses the experimental methods that were used to prepare, analyze, and test various approaches to improving adhesion between the hydrocarbon polymer and the fluoropolymer using the process technique known as plasma etching. The evaluation of these approaches required carefully controlled and designed experimentation, analytical analysis, and various methods of testing thin film adhesion. The first section introduces the test vehicle/device used for evaluation and the processing which was used to fabricate experiment samples. The following experimental design section details the layout of the experiments that were run for each approach and provides an understanding of the relevant factors to be evaluated for each case. The next section provides perspective on the surface analysis testing performed in-situ on substrates. This is followed by a discussion of the various analytical methods used to measure the various properties critical in the evaluation of thin film adhesion on experimental devices. A section detailing the specific methods utilized to perform destructive adhesion testing is included. The final section talks about the long-term product reliability requirements for optical communications devices and presents the test methods employed in the evaluations for this work.

3.2 Sample Processing

Total wafer cycle time required to fabricate polymer photonic ICs from polymer solutions is somewhere between three and five days depending on the microfabrication methods utilized. Full functional devices were processed using conventional microfabrication processing methods and equipment. Basic thin film stacks on substrates (experimental samples) were fabricated for tests in which the full waveguide structure was not required. Activation of the substrate surface was performed on select samples and not performed on others for comparison purposes. The process methods and details to perform device fabrication, Oxygen blanket plasma and RIE surface microfeature surface activation are presented.

3.2.1 Polymer Photonic Device Fabrication

Typical Photonic ICs are made by fabricating waveguide channels surrounded by cladding on a substrate as shown in Figure 3-1. Optical signals are coupled in to the core channel where they propagate via total internal reflection. The core index of refraction must be higher than that of the cladding index for light guiding to occur.

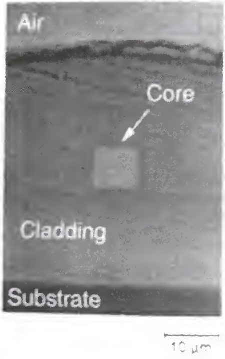

Figure 3-1. Cross section of a polymer waveguide device [26].

Various approaches exist for the fabrication of these waveguides including direct electron beam writing method, photoresist lift-off method, dry etching, and selective UV photoactivation method. For the purposes of this work, the dry etching method was chosen for waveguide fabrication which is shown in Figure 3-2.

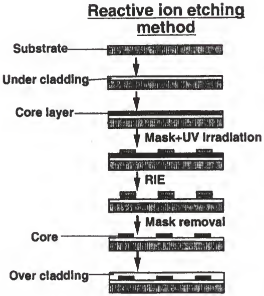

Figure 3-2. Reactive ion etching method for waveguide fabrication [27].

In this approach, conventional semiconductor fabrication techniques and equipment to perform thin film processing, photolithography, metallization, wet chemical processing, and plasma/reactive ion etching are employed. This approach is the most widely used and accepted primarily due the ability to produce very smooth and highly vertical core features. Control of the core profile and minimal surface roughness controls scattering losses and contributes to low loss device performance.

3.2.2 Experiment Sample Fabrication

Polymer substrates are prepared from bulk polycarbonate. These substrates can be cut from sheets or injection molded in to 100mm discs with single flat. Substrates are introduced in to a class 100 cleanroom environment for fabrication. All substrates are first immersed in IPA for 10 minutes to remove and organic residues that may be on surfaces. Selected wafers were subjected to plasma surface treatments as detailed in sections 3.2.2.1 and 3.2.2.2. For these etch treatments, wafers are processed using an Applied Materials(AMI) MxP+ etch chamber attached to a AMI Centura platform and controlled using AMI proprietary software. A simple schematic of the MxP+ chamber is presented in Figure 3-3.

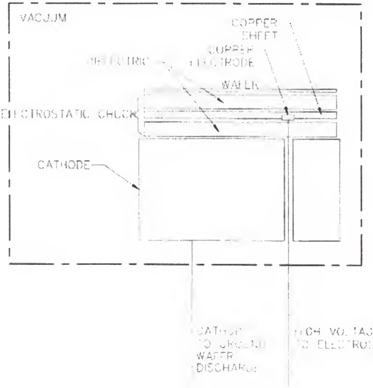

Figure 3-3. MxP+ etch chamber schematic [28].

Following plasma surface treatment, an undercladding thin film is deposited using the solution spin coating/casting method. This film is convection baked for 24 hours to evaporate and drive out all remaining solvents. Following this, full fabrication of polymer waveguides is performed according to the procedure in Figure 3.2. This process flow contains many trade secrets which are highly proprietary in nature and not directly relevant to this work. These methods are not be disclosed in this work.

3.2.2.1 Surface activation using oxygen plasma

Unpatterned samples were individually subjected to an RF plasma oxygen gas discharge in the chamber shown in Figure 3-3. Power, pressure, and time were varied. The chamber wall and cathode temperature were kept constant for all samples at 35°C. Since the chamber was configured for 150mm wafers, a special holder had to be used consisting of a 150mm silicon wafer with a 25mm polycarbonate donut ring affixed to allow processing of our 100mm substrates.

3.2.2.2 RIE surface microfeature formation

All experiment processing was performed in a cleanroom environment rated to better than class 100 standards. Polycarbonate substrates were rinsed in IPA for 5 minutes, DI water for 5 minutes, and spun dry for 5 minutes. For this treatment, wafers required an etch resistant mask applied to form the microstructural features. This was accomplished through metallization and photolithography. Prior to metallization, all wafers received blanket oxygen plasma etch treatment for 300sec. At 75W and 75mtorr to activate the surface for aluminum deposition. All wafers were sputter deposition coated with .1μm aluminum on the plasma activated top surface. Wafers were then sent through photolithography where a photoresist was first deposited in the forma a thin film through spin coating and convection drying. Wafers were coated with .1μm positive acting photoresist by spin coating and soft baked in a convection oven at 90°C for 15 minutes. Next, a mask was placed in contact with the photoresist covered surface and subjected to ultraviolet light to selectively cross-link the photosensitive polymer. Wafers were exposed using the appropriate mask (5x5μm or 10x10μm) according to the experiment layout in Figure 5-1. Wafers were developed and dried. Following this, the metal was etched using an acid bath composition of phosphoric, nitric, and acetic acids. The resulting masked wafer was then sent through the Applied Materials MxP+ dielectric etch chamber. The same silicon/polycarbonate donut ring fixture was used to transport wafers as explained in the previous section (3.2.2.1).

3.3 Experimental Design

The experimental design for each case was developed using JMP Statistical discovery Software (Version 4). For each treatment case, a screening experiment was first developed and then executed. Following on the conclusions from this initial screening experiment, a full or partial factorial experiment was developed and executed to find the optimal processing condition set.

3.4 Analytical Surface Analysis

Surface analysis was performed in attempt to understand and explain the results generated from the experiments. Analysis using utilizing the methods of optical microscopy, scanning electron microscopy (SEM), atomic force microscopy (AFM), stylus profilometry, contact angle measurement, Fourier Transform Infrared Spectroscopy (FTIR), and x-ray photoemission spectroscopy (XPS) were utilized.

3.4.1 Optical Microscopy

Optical Microscopy using a PolyVar brand microscope was utilized to perform investigation for thin film delamination of devices. 25mm x 40mm devices were singulated from 60 mil thick fabricated substrates using a standard manual Buehler wafer saw. For polymer devices, the dicing operation was found to leave a cut surface with a polymer lip from the heat generated during cutting. Samples edges were microtomed using a manual microtoming tool with a stainless steel blade to both remove the polymer lip and to provide a smooth edge surface for low loss fiber coupling to the device.

Samples were investigated at 50x magnification in bright field light reflection mode. A nomarski light polarizer was used to provide contrast between the thin film stack and the substrate. Images were captured using a standard CCD camera connected to the optical column of the microscope. Captured files were processed using standard photo editing software to normalize final color and contrast for comparison purposes.

3.4.2 Scanning Electron Microscopy

Scanning Electron Microscopy was used to generate three dimensional images and to visualize surface morphology. A JEOL JSM5900LV was used for all SEM analysis. Devices were singulated from substrates using a standard manual Buehler wafer saw. For polymer devices, the dicing operation commonly leaves a cut surface with a polymer lip from the heat generated during cutting. Edges were microtomed for approximately 20 mils. All samples were coated with 10-20 angstroms Au/Pd alloy using a table top SPI brand sputter coater. Samples were mounted on aluminum mounting fixtures using conductive tape on the back sides of the samples and on the corners. The system was used in high vacuum mode at base pressure on the order of 300mtorr. Electron beam energy of 5keV was used with a spot size of 20mm. Images were captured using the highest capture resolution available with no post modification of the micrograph image.

3.4.3 Atomic Force Microscopy

Atomic Force Microscopy micrographs were generated for detailed topographic analysis of the etched surface. These images were obtained using a Digital Instruments Nanoscope schematically represented in Figure 3-4.

Samples were affixed to a circular thin metal disc mount using tacky glue. 10mm x 10mm square samples were prepared using a standard manual dicing saw. The mounted samples were placed on a magnetic mounting platform for analysis. The

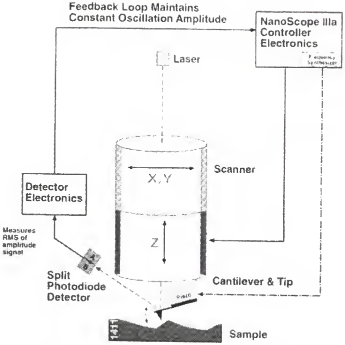

Figure 3-4. Digital instruments AFM equipment configuration schematic [29].

micrographs were taken in the tapping mode with silicon tips manufactured by Hitachi. At times, multiple images were taken from neighboring locations on the sample to ensure that the scan image was representative of the actual surface instead of an abnormal surface artifact or instrument setting.

Images were electronically captured and subsequently analyzed using digital instruments image analysis software. The "flatten" command was used on all images before any analysis was performed. This command was used to correct for curvature (non-flatness) of the sample. In many cases, sample non-flatness was found to be due to nonuniformity of the tacky glue or lack of full contact between the tacky glue and the sample in some areas.

First, a 3-D plot was produced from the data showing x, y, and z axes to scale. Next, a roughness analysis was performed on the data which provided RMS surface roughness, average surface roughness, and total surface area measurements.

3.4.4 Stylus Profilometry

Stylus profilometry was used to provide both step height data and large scale surface roughness measurement. Measurements were made using an Ambios model XP-2 stylus profilometer equipped with a 1μm radius stylus tip. Samples were prepared by mounting to a silicon wafer using double sided tape. Samples were scanned using .05mm/s scan speed, 20,000 data points of capture per second, and a scan length of 5mm. During the scan, a protective cover was used to eliminate any external environmental effects on the scan. This was necessary especially due to the fact that the equipment was located inside of a cleanroom where a high volume of air flow is present. The resulting x and z data was captured and plotted on a graph. A level function in the software was used to level the data. Manually positioned cursors were used to identify and to measure the step height of interest. To obtain surface roughness results, cursors were used to highlight the region of interest on the x-z plot. A special algorithm was used to analyze the data from this region and to provide an RMS surface roughness value. The length of the selected region for surface roughness evaluation was chosen to be 3 mm for all roughness analyses.

3.4.5 Contact Angle Measurement

Contact angle measurements were performed using an SL Industries comparator as shown in Figure 3-6 with image capture from the monitor using a digital camera. Contact angle values are usually attributed to both surface roughness and inhomogeneous composition. The measurement is shown in Figure 3-5 where γ is the surface free energy (surface tension), the subscripts S, SL, and L refer to the solid, solid-liquid, and liquid surface tensions respectively, and θ is the contact angle.

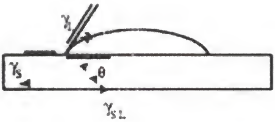

Figure 3-5. Contact angle measurement [30].

Measurement required an apparatus as shown in Figure 3-6 to capture the two dimensional profile of the water droplet in contact with the surface. For our purposes, a sessile drop test was performed in which the contact angle was measured with the water droplet held at steady volume. The substrate to be tested was placed on the stage between the light source and the microscope. A 10 ml syringe was used to deposit a 1 ml droplet of deionized water on the surface of the substrate sample. The stage was manipulated in the x, y, and z directions to position the edge of the water droplet appropriately in line with the light source and microscope. Adjustment of the light source as well as sources of secondary lighting was optimized to provide the appropriate contrast for subsequent image analysis. Digital images were taken from the monitor

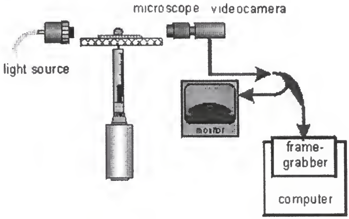

Figure 3-6. Contact angle analysis configuration [31].

output image. These digital files were measured on a computer system using image analysis and measurement software.

3.4.6 X-Ray Photoelectron Spectroscopy

Information about the surface chemistry of both treated and untreated samples was obtained using X-Ray photoelectron spectroscopy (XPS) – also commonly referred to as electron spectroscopy for chemical analysis (ESCA). XPS spectra were taken using a non-monochromated Aluminum Kα X-ray source. These photons interact with the atomic electrons primarily via the photon absorption process. The photoelectric process is the direct signature of the photon interaction with the atom and is the basis of this technique. A typical configuration similar to the system used in this work is shown in Figure 3-7.

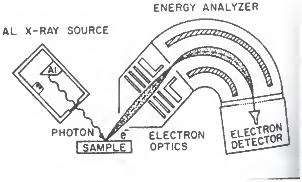

Figure 3-7. Typical XPS analysis configuration [32].

Analysis of XPS data required the utilization of references for interpretation. References were obtained from standard XPS data sources. The following molecular model for A-Bisphenol polycarbonate in Figure 3-8 and corresponding intensity peak data presented in Table 3-1 was used as the reference for the XPS data analysis chapters 4 and 5. This information was provided to compare to the bulk sample which was obtained by cutting in to the polycarbonate while under vacuum.

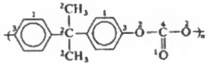

Figure 3-8. Molecular model for A-Bisphenol polycarbonate.

Table 3-1 Analytical data model for A-Bisphenol Polycarbonate XPS analysis

Atom	BE (eV)	Fwhm	Area %
C_{1s} 1 (Ring)	284.50	0.94	59
C_{1s} 2 (Methyl)	285.00	1.02	22
C_{1s} 3 (PhiO)	286.24	0.95	11
C_{1s} 4 (Carbonyl)	290.44	1.12	8
O_{1s} 1 (Carbonyl)	532.33	1.30	34
O_{1s} 2 (Ether)	533.97	1.32	66

3.4.7 Fourier Transform Infrared Spectrometry (FTIR) with Horizontal Attenuated Total Reflectance (HATR)

Conventional FTIR analysis using a Perkin Elmer Instruments Spectrum One analyzer was performed as a compliment to XPS in the effort to obtain chemical bonding information for surface species. Full substrates were analyzed by scanning and comparing a treated sample with a control(untreated) sample scan. The treated sample was that substrate which received a plasma treatment. An untreated sample did not receive a plasma etch treatment. Measurements on plasma treated samples were performed within a critical time of lass than one hour to avoid any effects from surface recombination and contamination. For FTIR analysis, IR radiation is split in to two beams as shown in Figure 3-9. One beam is of fixed length, the other of variable length. The varying distances between two pathlengths results in a sequence of constructive and destructive interferences and hence variations in intensities: an interferogram. Fourier transform converts this interferogram from the time domain into one spectral point on the more familiar form of the frequency domain.

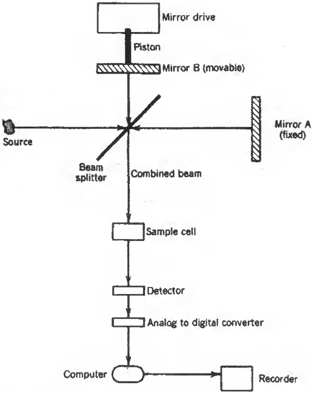

Figure 3-9. FTIR analysis equipment configuration [33].

To provide surface composition analysis, the Spectrum One FTIR analysis tool was equipped with a Horizontal Attenuated Total Reflectance (HATR) sampling accessory. This accessory provides a method for using FTIR to analyze surface properties of various materials including solids, powders, pastes, gels, and liquids. The ability to sample a surface instead of sampling by traversing the beam through the material is the primary advantage of HATR. A schematic showing the operating principle of HATR is presented in Figure 3-10. The figure shows an incident beam and an exiting beam at 45 degree angle to the sample. This orientation of the incident beam provides total internal reflection with the crystal. In the context of Figure 3-9, this HATR sampling accessory is the sample cell. This is the only difference between FTIR and FTIR with HATR.

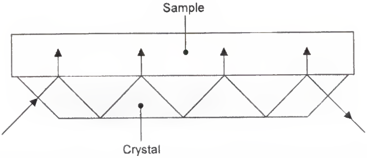

Figure 3-10. Horizontal attenuated total reflectance sampling method for FTIR.

The HATR technique is non-destructive. A sample is placed on top of a crystal with a high refractive index. In our case, a ZnSe (Zinc Selenide) crystal with a refractive index of 2.4 was used. "An infrared beam from the instrument is passed into the accessory and up into the crystal. It is then reflected internally along the crystal, and back towards the detector which is housed within the Spectrum One. Each time the beam is reflected within the crystal, it penetrates into the sample by a few microns. Figure 3-10 illustrates this process" [34].

Samples were analyzed in the spectral frequency range between 650cm^{-1} and 4000cm^{-1} with a resolution of 4cm^{-1} at a scan rate of .2 cm/s. Data was collected, normalized, and displayed as percent transmission vs. frequency.

3.5 Adhesion Testing

Adhesion testing of polymer thin films on polymer substrates in a relatively unestablished territory in the adhesion testing world. Samples were tested utilizing the most relevant adhesion testing standards and methodologies presently available. There are a number of methods used to test adhesion including the tape test, the peel test, and the scratch test. The scratch test was used for our experiments because it proved to be the most accurate method of adhesion evaluation for the material system being investigated.

Results obtained using this method are quantifiable with guideline standards available from recognized and accepted standard publishing companies such as ISO and ASTM.

Scratch test results were obtained using an Elcometer model 107 cross hatch cutter blade as shown in Figure 3-11 and associated hand tool/sample analysis kit. The cross hatch test is a method designed to determine the adhesion properties of a coating or thin film. The technique was originally developed as a method for adhesion testing of paints. Having selected the appropriate cutter blade tooth spacing – as specified based on coating thickness according to the manufacturer's specification contained in Appendix A, a cut of approximately 20 - 30mm (1 - 1.5") long was made while ensuring that enough force is used to cut all the way down to the substrate. A similar length cut was made at a 90° angle with the first cut - again, ensuring that the cut is all the way down to the substrate. The cut coating was brushed slightly with a soft brush or tissue to remove any detached flakes or ribbons of coating, then the resulting cross-hatch pattern was checked according to the Classification of Adhesion Test Results - as described in standards ISO 2409 or ASTM D3359. An adhesive tape rated in compliance with these standards was used prior to checking the result to remove loosened debris. Results were visibly inspected and rated according to the standard specification scale between 0 and 5 (0 being best adhesion – no flaking, 5 being worst - large scale and wide-spread flaking).

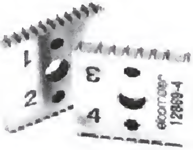

Figure 3-11. Elcometer model 107 cross hatch cutter blades.

3.6 Environmental Performance Testing

Reliability testing is composed of a set of environmental test conditions which must be passed to ensure that the materials used in the product are capable of performing as designed and at the performance levels expected under a wide range of operating conditions. This testing is common in high tech electronics and optics. Optical devices such as those being evaluated in this study commonly require certification to industry standards known as Telecordia. Telecordia test specifications spell out specific tests and parameter ranges for which products must successfully pass. These tests typically include damp heat (85°C - 85%RH) and temperature range cycle testing. Telecordia specification compliant testing was performed for both damp heat and temperature cycle testing. These tests are the most effective and accurate method for testing the properties of adhesion and for comparison of the effectiveness of the various adhesion enhancement processes developed in this work. These tests do not necessarily provide lifetime information since they do not always result in failure. To understand adhesion failure and to provide estimations of product lifetime, accelerated test methods can be employed. Accelerated testing methods of boiling/ice water bath immersion and pressure cooker tests were used to predict performance for very long term exposure and to predict product operating lifetime.

3.6.1 Temperature Cycling Test

Samples were placed in 10cm diameter polypropylene dishes and set in an Inspec temperature cycling oven on the bottom (floor) level steel surface. The oven was programmed to repeatedly execute the thermal cycling profile shown in Figure 3-12 for a total of 300 cycles. A single cycle consisted of placing samples in the oven at room

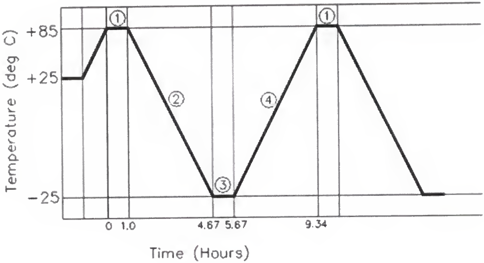

Figure 3-12. Temperature cycling program profile.

temperature and ramping the oven to 85°C. Samples were held at 85°C for one hour. Slow cooling was performed at a rate of .4°C/min to a temperature of -25°C. Samples were held at -25°C for 1 hour. Following this, samples were heated at a rate of .4°C/min to 85°C to complete the cycle. Upon test completion, samples were removed and stored in a nitrogen dry box pending inspection.

3.6.2 Accelerated Thermal Shock Testing

This test was performed using water as a means for efficient/fast transport of thermal energy to the device to enable very rapid heating and cooling. The exposure to water in this test must be considered when conclusions are made using these test results as it may be difficult to separate out the thermal effects from that of the water in the delamination event.

3.6.3 Damp Heat (85°C - 85%RH) Test

A BlueM reliability test chamber was used to perform the damp heat test. Samples were placed in polypropylene dishes as in section 3.6.2 and set in to the oven on the stainless steel shelf in the middle of the chamber. The Oven was programmed to ramp up to the setpoint of 85°C and 85%RH in a period of less than 5 minutes. The program was set to maintain these conditions for 1000 hrs of testing. Upon test completion, samples were removed and stored in a nitrogen dry box pending inspection.

3.6.4 Accelerated Moisture/Temperature Testing

For this test, a Mirro brand 10 inch diameter domestic pressure cooking vessel was used. An 8 inch diameter by 4 inch height Pyrex® glass dish was placed upside-down in the vessel to provide a raised platform upon which samples in a three inch diameter shallow height Pyrex dishes were placed. One inch of tap water was added to bottom of the vessel to create an extreme damp heat environment. The vessel was heated on a laboratory hot plate at a temperature of 200°C. Samples were periodically tested by removing the vessel from heat, releasing the steam pressure, and allowing the samples to cool and dry prior to inspection.

CHAPTER 4
SURFACE ACTIVATION USING OXYGEN GAS PLASMA

A plasma etching chamber with oxygen feed gas was chosen and evaluated for its predicted high degree of effectiveness in altering the surface properties of the polycarbonate substrate prior to fluoropolymer thin film casting for waveguide fabrication. It is well known that oxygen plasma processing can be highly effective in surface property modification of various materials by either oxidation or reduction reactions. The ability to alter surface properties of polymers using plasma environments has been reported for a number of systems to improve wettability. Nitrogen, argon, and oxygen plasmas have each shown to be effective in lowering surface contact angles [35]. In comparison, oxygen is generally demonstrated to be the most effective plasma environment for enhancing surface wettability. There is reason to believe that oxygen plasma etching is one of the most effective means for polymer surface modification of plastic materials. Aggressive oxygen environments are likely most effective due to their unique ability to create dangling bonds and increase surface roughness/area. For the system under evaluation for this work, the effectiveness of the treatment method will depend on the capacity of the fluoropolymer thin film to be affected by van der Waals/dipole intra-molecular bonding mechanism.

4.1 Background

The use of plasma etch surface treatment to enhance adhesion is reported commonly in the literature [36,37,38]. Plasma treatment can be performed in a highly reactive mode capable of both physical and chemical attack. Oxygen is used commonly to etch polymer materials due to its high chemical reactivity with both carbon and hydrogen. Fluorinated gasses can also be used to etch polymers. They are frequently used to control the etching rate, selectivity, and sidewall profiles in the case of patterned etching.

Etched surfaces typically exhibit very different surface energy levels compared to that of the untreated sample. Surface activation through plasma etching is an effective method for producing a high energy surface. High energy surfaces have been shown to improve the level of adhesion of thin films.

Adhesion enhancement of polymers using plasma processing is an attempt to enhance the overall bond strength between two surfaces by altering the surface to be adhered to. The stronger the bond mechanism - the better the adhesion will be. The most attractive route to accomplish this would be to create chemical bonding between the materials (chemisorption). This approach would involve the modification and creation of functional groups on the material surface that would chemically react with the second material. Although this approach is promising and theoretically very promising, the chemistry involved is not in the scope of this research. The alternate approach which we are concerned with focuses on van der Waals or dipole forces of attraction (physisorption) and the enhancement of this mechanism for improved adhesion.

When bulk material or thin film surfaces are discussed, it is recognized that they are capable of possessing an associated free surface energy level. This surface energy is a primary function of the surface monolayer molecules and their associated level of polarity. Polar surface molecular bonding such as the case of C-O will provide van der Walls forces leading to a ‘high energy surface’. Non-polar molecular bonding such as the case of C-F will have very little free energy which will result in a much low free energy surface property.

As high energy surfaces provide higher aggregate effective dipole moments or bonding forces, these surfaces are more desirable for adhesion purposes. The higher free surface energy levels are more highly capable of bonding with a second surface. High free energy levels correlate to higher bond strength and thus better adhesion.

Common plastics exhibit a wide range of surface energy properties as shown in Table 4-1. The very low surface energy of fluoropolymers (due to the very high C-F bond strength) is the fundamental reason for the use of these materials, such as Teflon (PTFE), in non-stick applications such as cookware.

Table 4-1. Surface energy values of common plastic materials [39,40].

Material	Formula	Critical surface tension, dyne/cm
Polycarbonate	$-OC_6H_4-C(CH_3)_2-C_6H_4-O(CO)-$	46
Polyethelene	$-CH_2-CH_2-$	31
Polyvinyl fluoride	$-CH_F-CH_2-$	28
Polytrifluoroethelene	$-CF_2-CHF-$	22
Polytetrafluoroethylene (PTFE)	$-CF_2-CF_2-$	18

This table shows that the surface energy of the Polycarbonate structure, shown in Figure 4-1, is much higher than the fluoropolymer material (PTFE). This phenomenon is due primarily to the highly polar C-O and C-H bonding in Polycarbonate in contrast to more highly non-polar characteristic of the C-F bond in PTFE.

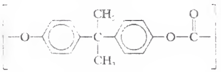

Figure 4-1. Molecular structure of A-Bisphenol polycarbonate [41].

Since molecular structure has a significant effect on surface energy, it is reasonable to predict that there exists a strong capability to change a material's surface energy by altering the molecular structure of its surface. Plasma etching has been commonly used to change surface structures as plasmas are quite effective in their ability to break both inter and intra molecular bonds via highly energetic radicals. The new surface creates a fertile environment for the formation of new/different bond groups via highly chemically reactive surface species with a strong tendency to reduce total free energy by new bond formation.

The change in surface energy due to plasma processing can be measured both directly and indirectly by various methods. The effectiveness of plasma treatment can not be adequately quantified using direct surface energy measurements since these measurement techniques are not accurate above 73 dynes/cm. In almost all cases, plasma treatment increases surface energy beyond this threshold. Results can best be measured using contact angle measurements as described in section 3.4.5. Table 4-2 shows contact angle measurements for various plastics and the change in angle due to plasma treatment.

Table 4-2. Untreated/plasma treated contact angle measurements for various polymers [42].

Material	Initial water contact angle (degrees)	Post plasma treatment water contact angle (degrees)
Polycarbonate	90	20
Polyethelene	87	42
Polyvinyl fluoride	78.5	36
Polytrifluoroethelene	92	53
Polytetrafluoroethylene (PTFE)	96	68

Beyond surface energy properties, there exist additional factors which must be considered as potential contributors to adhesion. These factors include surface roughness, post process molecular surface reorganization, and impurity migration among others. These factors and the extent of their contribution should be investigated and accounted for (where possible) since the end goal is to develop a process for long-term device reliability. Surface roughness can be quantified using both profilometry and atomic force microscopy. Long-term environmental testing and lifetime extrapolation as performed in Chapter 6 is the most effective assessment method to identify and understand the potential impact of molecular structure changes due to process holding and device ageing.

Polymer etching is more limited in the range of process conditions that are available due primarily to heat generation concerns. Unlike conventional materials processed in etching chambers and systems such as silicon and silica, polymers experience softening as a result of glass transition temperatures in the 100°C -200°C range. Polycarbonate, for example, starts warping at 153°C. This makes substrate temperature control a critical factor in the evaluation of these processes. For deep etching (>20μm), etching must be performed in sequences of 10 minutes with a cool down step after each etch step.

4.2 Results

For the purposes of evaluating the effect of blanket oxygen plasma treatment as a method for improving adhesion, a designed experimentation matrix was developed. A full factorial experiment was developed with one center point and one control condition. The control condition was that of the unetched polycarbonate substrate. Table 4-3 details the experimental design matrix and the plasma treatment condition factors which were evaluated. For the remainder of this chapter, samples will be referred to by their identification designation letter. This experimental matrix was designed to test the full

Table 4-3. Sample identification and plasma treatment conditions.

ID	Etch Time (sec)	Power (watts)	Pressure (mtorr)
A	160	40	40
B	160	40	160
C	160	160	40
D	160	160	160
E	660	40	40
F	660	40	160
G	660	160	40
H	660	160	160
I	300	80	80
J	0 (control)	0 (control)	0 (control)
K	80	80	80
L	160	80	80
M	660	80	80
N	1000	80	80
O	2000	80	80
P	3000	80	80
Q	4000	80	80
R	5000	80	80

range of critical factors thought to have the greatest impact on the polymer etching. The factors of etch time, power, and pressure were chosen for evaluation. The range of values evaluated for pressure (40-160mtorr) was the full operating pressure regime available for the chamber equipped with a mass flow controller programmed to a setpoint of 100sccm O_2 gas flow. The power regime chosen was not due to equipment limitations. This power range between 40 and 160 watt was selected so as to limit the thermal energy buildup of the polymer substrate during etching to below 100°C. Using temperature dot tape, 160 watts was the maximum safe operating level to avoid thermal damage to the substrate. Careful attention to thermal management of the substrate was necessary to prevent substrate warping which starts to occur upon approach of the glass transition temperature of the material. The factor of time was evaluated in a full factorial matrix (160sec & 660sec) and also in a customized progressive series (80sec – 5000sec).

4.2.1 Structural Characterization

4.2.1.1 Profilometry

Agarwal et. al. has reported that unlike dielectric, metals, or semiconductor materials, polymers experience significant surface roughening at the surface on the etching front. As polymers such as polyimide are etched under typical low pressure (20-40mtorr) conditions in an oxygen gas plasma, the etching surface becomes rough and the degree of roughness exhibits a primary correlation to the total etch depth [43]. These results are presented in Figure 4-2. Initial work in this study on polycarbonate found this same phenomenon and relationship to also exist.

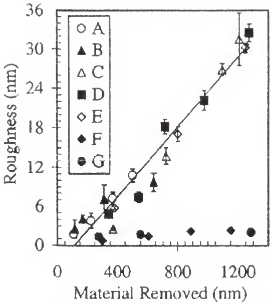

Figure 4-2. Surface roughness evolution during oxygen etching of polycarbonate [44].

Further verification of the existence of this etch roughness evolution phenomenon was performed in part using profilometry. Profilometry was used to measure etch depth and etch rates for the various power/pressure regimes evaluated in the experimental matrix detailed in Table 4-3. The resulting etch depth and etch rates are presented in Figure 4-3 and Table 4-4.

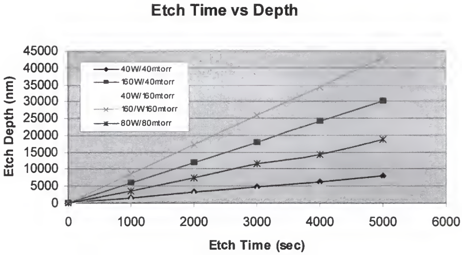

Figure 4-3. Polycarbonate material removed vs. oxygen etch time.

Table 4-4. Material removed at constant power and pressure

Power(Watt)/Pressure(mtorr)	Material Removed (nm)	Etch Rate (nm/s)
80W/80mtorr	3692	3.69
40W/40mtorr	1600	1.60
160W/40mtorr	6000	6.00
160W/160mtorr	8600	8.60
40W/160mtorr	1300	1.30

The roughness results were obtained using atomic force microscopy as are discussed in section 4.2.1.2. Samples were prepared and measured according to the procedure for profilometry analysis detailed in section 3.4.3. A step height was created using a 1000Å sputtered aluminum mask and photolithography. A straight line patterned chrome mask was chosen for photolithography. The mask provided regularly spaced measurement features 10μm wide with a 50μm pitch. Samples were prepared through metal mask deposition and photolithography patterning. The aluminum mask was etched using a standard metal acid etchant and dry etched according to the conditions in Table 4-4. Samples were soaked in acid etch to remove the aluminum mask and measured. This patterning process was necessary to enable the measurement of etch depth using profilometry. This technique was chosen instead of thin film interferometry which is commonly used and much less complex for thin and thick film measurements. This film interferometry is not capable of measuring thick substrates such as those used in this work on the order of 60 mils in thickness.

The etch rate data obtained in Table 4-4 was useful for extrapolation throughout this work. Using these results, etch depths were calculated for the experimental samples in Table 4-3. The results are shown in Table 4-5.

Table 4-5. Experimental matrix sample etch depths.

ID	Etch Time (sec)	Power (watts)	Pressure (mtorr)	Etch Depth (nm)
A	160	40	40	590
B	160	40	160	208
C	160	160	40	960
D	160	160	160	1,376
E	660	40	40	1,056
F	660	40	160	858
G	660	160	40	3,960
H	660	160	160	5,676
I	300	80	80	1,107
J	0 (control)	0 (control)	0 (control)	0 (control)
K	80	80	80	295
L	160	80	80	590
M	660	80	80	2,435
N	1000	80	80	3,690
O	2000	80	80	7,380
P	3000	80	80	11,070
Q	4000	80	80	14,760
R	5000	80	80	18,450

4.2.1.2 Atomic force microscopy

Tapping mode atomic force microscopy as outlined in section 3.4.2 was used to characterize the surface morphology of the etched and unetched polymer surfaces for Table 4-3 experiment samples. Only by AFM inspection, small scale roughness can be seen. This is in comparison to the technique of profilometry measurement and analysis.

Profilometry provides measurements over a span of hundreds of microns to thousands of microns. AFM is used to precisely analyze small scale roughness over areas less than 15 μm^2. These AFM measurements provide insight in to the presence or creation of very small scale roughness that may be present. Experiment samples were analyzed using AFM technique with a scan rate of 0.56 Hz and a scan size of 3µm. Careful attention was given to voltage and gain settings. These parameters were adjusted for each sample to suppress their influence on analysis results.

Figure 4-4 presents the AFM produced image of the virgin polycarbonate surface. This baseline image is important to allow for comparison as we can see that the unetched surface itself shows some degree of roughness. Inspection of the micrograph of the surface shows surface striations which are most likely due to the sheet rolling process used to produce the material from which these substrates were cut. This appearance of wound string on the surface is widely reported in the literature. AFM results for the etched surfaces are presented in Figure 4-5(a-d) which provide a comparison for samples under conditions of constant time with variable pressure and power.

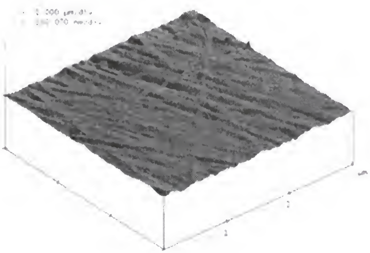

Figure 4-4. AFM micrograph of virgin polycarbonate surface

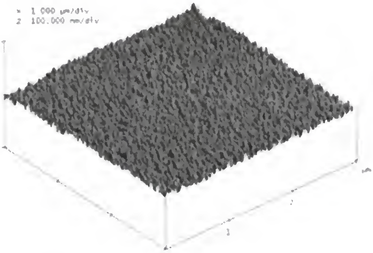

(a) Sample E - 660 sec., 40W, 40mtorr

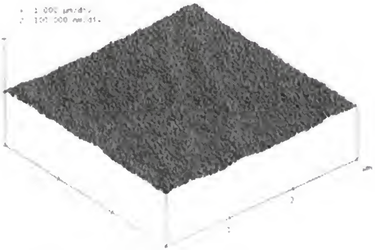

(b) Sample F - 660 sec., 40W, 160mtorr

Figure 4-5(a-d). AFM analysis at Constant Time/ Variable Pressure and Power

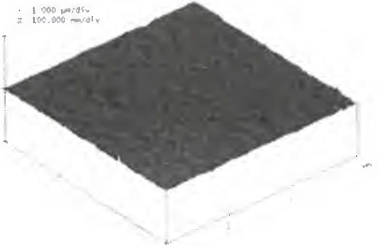

(c) Sample G - 660 sec., 160W, 40mtorr

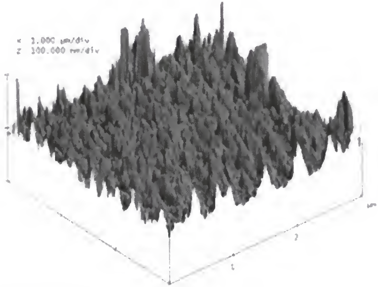

(d) Sample H - 660 sec, 160W, 160mtorr

Figure 4-5(continued)

The preceding images taken at constant etch time (660 sec) provide a quick comparison of the different power and pressure regimes and their resulting affect the surface morphology. These images show a wide range of surface roughening. High power and pressure conditions (160watt / 40mtorr) produced the smoothest surface of all samples. This surface is better than that of even the pre-etched surface. The conditions of high power and pressure (160watt / 160mtorr) show an extremely rough surface with cratering. The two low power conditions (40watt) show finely distributed roughness with the low pressure condition slightly more impressive than that of the high pressure sample. All conditions showed a small scale roughening when compared to the unetched polycarbonate surface. The small scale roughening has characteristics of sharp topography changes while the untreated sample roughness is much less abrupt in appearance

One drawback is that these images do not take the effect of etch time or etch depth due to etch rate differences among the pressure and power regimes. It is well known from the literature that there is a roughness evolution which occurs as polymers are etched for longer durations. The differences in etch rate combined with the known phenomenon of etch roughness evolution present cause for concern that the conditions of constant time with variable power and pressure can be confounded. Due to this concern, the effect of etch time and etch depth (if any) shall be examined through AFM micrographs (presented in the following sections) and taken in to account where possible in the final analysis of these results. Figure 4-6(a-d) provides a comparison of samples for which power and pressure were held as constant factors (80watts and 80mtorr) with etch time as the variable factor (80sec – 5000sec).

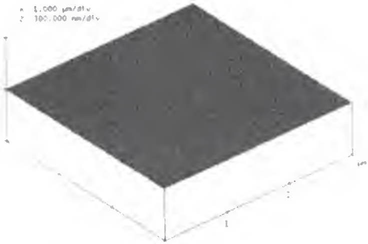

(a) Sample K – 80 sec., 80W, 80mtorr

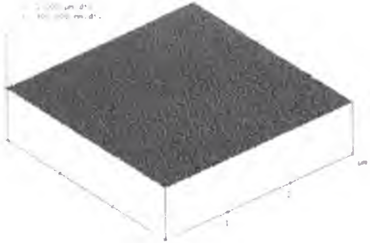

(b) Sample L – 160 sec., 80W, 80mtorr

Figure 4-6(a-h) AFM analysis at Constant power and pressure

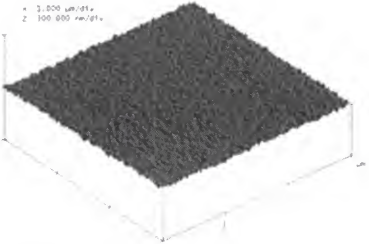

(c) Sample M – 660 sec., 80W, 80mtorr

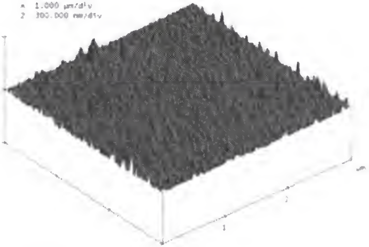

(d) Sample N – 1000 sec., 80W, 80mtorr

Figure 4-6(continued)

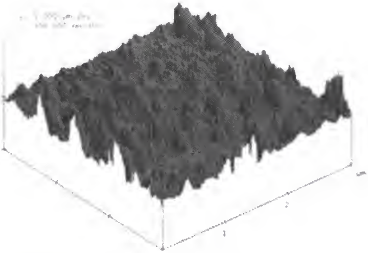

(e) Sample O – 2000sec., 80W, 80mtorr

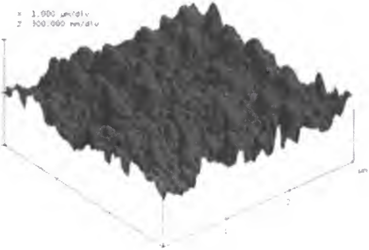

(f) Sample P – 3000 sec., 80W, 80mtorr

Figure 4-6(continued)

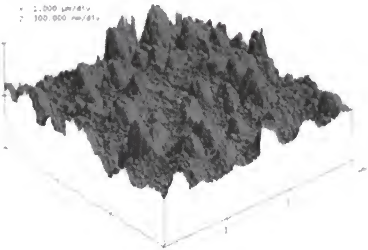

(g) Sample Q – 4000 sec., 80W, 80mtorr

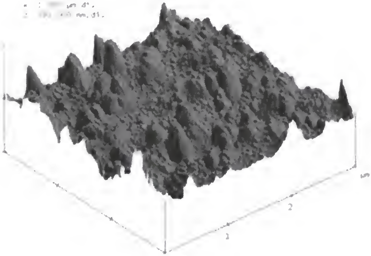

(h) Sample R – 5000 sec., 80W, 80mtorr

Figure 4-6(continued)

Data analysis was performed on the captured data from each AFM analysis to provide qualitative measurement information to use in comparison between samples and for use in DOE results modeling. Output from the analysis included RMS surface roughness, average surface roughness, and surface area. Table 4-6 is a summary of the AFM image analysis results obtained. RMS roughness and surface area are shown for all samples. The results are presented in a table format here. Following this is a graphical presentation of the core matrix experiment (Samples A-I) presented in the form of main effect factor interaction plots for further analysis.

Table 4-6. AFM roughness measurement data summary.

ID	Etch Time (sec) /Power (watts) /Pressure (mtorr)	RMS Surface Roughness (nm)	3μm^2 Scan Surface area (μm^2)
A	160 /40 /40	3.03	9.44
B	160 /40 /160	2.05	9.21
C	160 /160 /40	2.89	9.35
D	160 /160 /160	4.98	9.77
E	660 /40 /40	3.62	9.43
F	660 /40 /160	2.39	9.10
G	660 /160 /40	1.21	9.06
H	660 /160 /160	15.04	10.54
I	300 /80 /80	6.98	10.16
J	0 (control)	1.78	9.05
K	80 /80 /80	1.70	9.41
L	160 /80 /80	2.78	9.75
M	660 /80 /80	6.77	10.85
N	1000 /80 /80	11.48	12.12
O	2000 /80 /80	32.42	13.13
P	3000 /80 /80	38.51	11.69
Q	4000 /80 /80	40.94	11.77
R	5000 /80 /80	37.72	11.25

The Root Mean Square (RMS) roughness presented here is the standard deviation of the measured Z values within a given area. RMS function analysis represented as:

$$\text{RMS} = \sqrt{\frac{\sum_{i=1}^{N}(Z_i - Z_{ave})^2}{N}} \tag{4.1}$$

The use of RMS data measurement is a standard metric used to quantify surface roughness. The same data can also be analyzed to calculate values of surface area. From the data in Table 4-6, factor interaction plots can be generated for roughness and surface area analysis as presented in Figures 4.7 and 4.8.

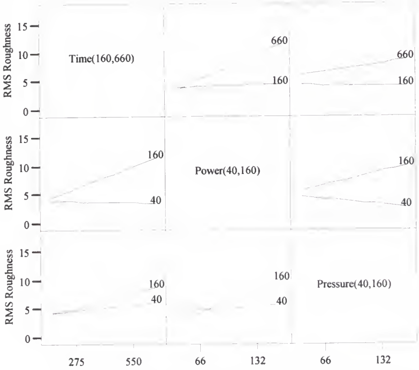

Figure 4-7. RMS roughness etch factor interaction profiles for variable etch time, power and pressure conditions.

The previous experiments from Table 4-5 were intended to provide insight in to the individual factors of etch time, power, and pressure on the surface morphology. The results indicate that there exists a wide variation of roughness and surface area results within the range of factors evaluated. One additional factor of suspect importance is total etch depth. Total etch depth is not the same as total etch time. Variations in etch rate when dissimilar power and pressure regimes are used present different total etch depth results at constant etch time. It is important to attempt to decouple and characterize the two factors independently.

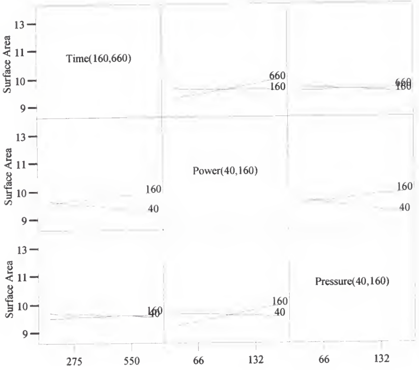

Figure 4-8. Surface area etch factor interaction plots for variable etch time, power and pressure conditions.

In the effort to understand total etch depth effects, the experiment in Table 4-7 was performed. All five wafers (identified as IDs S-W) were etched to a depth of 2,000nm.

Table 4-7. Constant etch depth experiment matrix.

ID	Etch Time (sec)	Power (watts)	Pressure (mtorr)	Etch Depth (nm)
S	1,351	80	80	2,000
T	3,125	40	40	2,000
U	833	160	40	2,000
V	581	160	160	2,000
W	3,846	40	160	2,000

Etch time was varied using the etch rate data obtained in section 4.2.1.1. Sample substrates S-W were prepared and analyzed using AFM analysis as performed on Samples A-R. These five samples of constant etch depth were representative of the full range of power and pressure factors evaluated in this work. The target etch depth was 2,000nm. The etch time was calculated by dividing the target etch depth by the etch rate

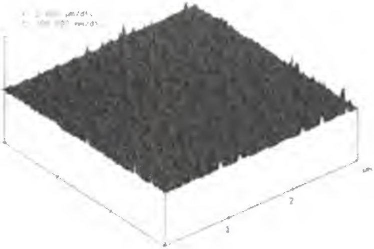

(a) Sample S - 80W, 80mtorr

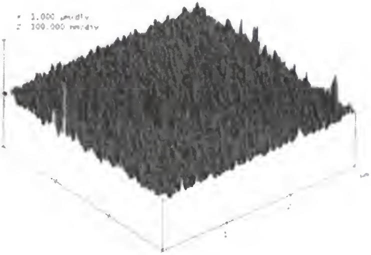

(b) Sample T - 40W, 40mtorr

Figure 4-9(a-e). AFM micrographs for constant etch depth; variable pressure and power.

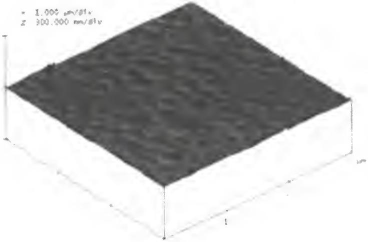

(c) Sample U - 160W, 40mtorr

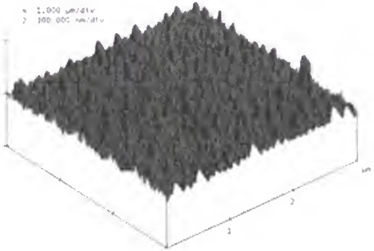

(d) Sample V - 160W, 160mtorr

Figure 4-9(continued)

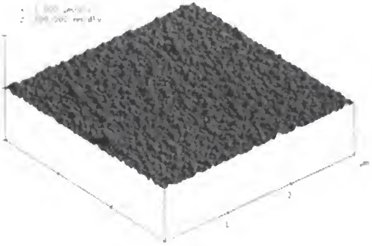

(e) Sample W - 40W, 160mtorr

Figure 4-9(continued)

as determined through profilometry and presented in Table 4-4. The resulting AFM micrographs of the surfaces are presented in Figure 4-9 for the five samples in Table 4-7. Sample U (160watt/40mtorr) shows minimal roughness when compared all other conditions S-W. This is consistent with those results observed in the previous matrix experiment in which sample G (660 sec/160watt/40mtorr) resulted in the absolute minimal surface roughness of all samples A-J. Sample V (160watt/160mtorr) showed the greatest roughness in comparison to those samples S-W. This is also very consistent with the findings among samples A-J which found sample H (660sec/160watt/160mtorr) to exhibit the most severe surface roughening. Table 4-8 details the AFM roughness and surface area measurement analysis results. For all five samples S-W etched to a constant etch depth, measurements of RMS surface roughness and surface area show drastic effects between plasma etch environment conditions. The results from this experiment

Table 4-8. AFM measurement data summary – constant etch depth roughness results.

ID	Etch Time (sec) /Power (watts) /Pressure (mtorr)	RMS Surface Roughness (nm)	3μm^2 Scan Surface area (μm^2)
S	1,351 /80 /80	8.32	10.49
T	3,125 /40 /40	6.74	10.19
U	833 /160 /40	2.94	9.13
V	581 /160 /160	18.22	16.79
W	3,846 /40 /160	5.85	9.44

fall in line with those expected when compared to those in Table 4-6. The results within Table 4-8 from the experiment in Table 4-7 are presented in the form of a factor interaction plot in Figure 4-10.

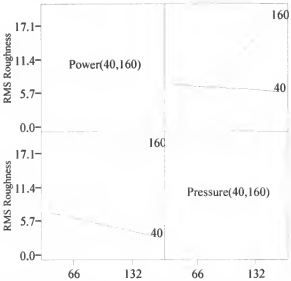

Figure 4-10. RMS roughness etch factor interaction profiles for constant etch depth conditions.

Atomic Force Microscopy was used to provide micrographs of the etch treated and untreated surfaces of polycarbonate substrates. This technique provided outstanding surface resolution as can be seen in the micrographs presented in this section. The results show a wide variation in surface conditions resulting from the range of plasma etching factors evaluated. In addition to the visual images produced, the technique also proved valuable in the production of detailed roughness analysis measurements to allow surface quality roughness and surface area quantification.

4.2.1.3 Contact angle measurement

Contact Angle measurements are used to assess the change in surface energy created on the substrate surface through the etching process. In this case, contact angle measurements provide a simple means of measuring the free energy at the surface for comparison between plasma treated and untreated samples. Figure 4-11 shows the result of the sessile drop test on our untreated polycarbonate substrates. The test shows a contact angle of approximately 75 degrees. This result is in close accord with those obtained and published by Hegemann et al. for untreated polycarbonate [45].

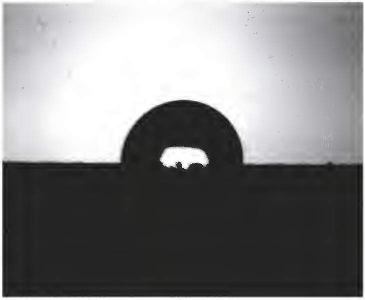

Figure 4-11. Untreated polycarbonate substrate sessile drop test.

Upon subjecting the substrate to oxygen plasma modification, the sessile drop test was again performed with much different results as shown in Figure 4-12. We can clearly see that there is a change in the contact angle from 75 degrees to approx. 20 degrees in this case. This change in contact angle is due to greater surface forces which are available to act upon the polar water molecules. Attractive surface dipole forces present from the surface structure have a net affect on water molecules within the droplet. These forces act upon the droplet to move it from the equilibrium minimal energy shape (circular).

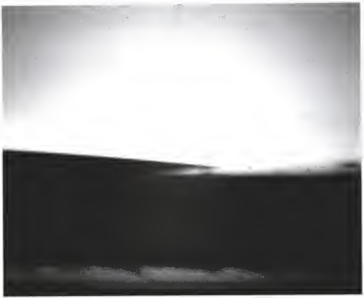

Figure 4-12. Oxygen treated polycarbonate substrate sessile drop test.

Contact angles were measured for sample A-J treatment conditions from the experiment in Table 4-3 according to the procedure for contact angle measurement presented in section 3.4.4. The results are presented in Table 4-7.

Table 4-7. Post treatment contact angle measurements for experimental matrix conditions.

ID	Etch Time (sec) /Power (watts) /Pressure (mtorr)	Average Contact Angle (degrees)
A	160 /40 /40	30
B	160 /40 /160	30
C	160 /160 /40	35
D	160 /160 /160	10
E	660 /40 /40	20
F	660 /40 /160	35
G	660 /160 /40	8
H	660 /160 /160	7
I	300 /80 /80	11
J	0 (control)	75

Sample J represents the untreated substrate with a water contact angle of 75 degrees. The lowest contact angle was realized under treatment conditions of 660 sec, 160 watts, and 160 mtorr conditions. This is the same condition which produced the highest RMS roughness and surface area value as discovered under AFM analysis. The extremely low contact angle of Sample G (660 sec/ 160 watt/ 40 mtorr power) is a surprising result. Sample G produced the smoothest surface of all samples A-J under AFM analysis.

Summation of the results can be most effectively presented in a main effects analysis plot. Main effects analysis of the plasma treatment factors against the responses observed and reported in Table 4-7 are presented in Figure 4-13. At the factor center points as shown by the dotted vertical lines, a contact angle of 20.5 degrees is predicted. Lower contact angles are realized most evidently by increasing the power level. Increasing the etch time also will lower the contact angle but to a lesser degree than changing power. Pressure seemed to have very little effect of the contact angle.

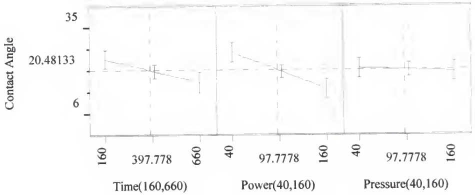

Figure 4-13. Main effect analysis for contact angle measurements

4.2.1.4 XPS

XPS analysis was performed on a limited set of samples to generate an understanding for the fundamental mechanism by which polycarbonate is etched in a plasma environment. Information which provides molecular structure at the surface is obtained through chemical bond detection. XPS is very effective in detecting chemical bond energy information at the near surface of polymers and providing quantification of these bond structures. This information is helpful in the analysis of various other test methods and in the formulation of theoretical explanation for adhesion performance under various treatment conditions.

Three samples were prepared and sent for XPS analysis. Samples labeled 'clear' and 'etched' were prepared from the same wafer by placing a 10cm x 10cm mask from cleaved silicon wafers on a plastic substrate and subjecting this wafer to the plasma etch control condition (condition I - 300sec, 80W, 80mtorr). The clear sample was taken to be that section of the wafer protected by the silicon mask while the etched sample was taken from an unprotected area. For reference, a fresh sample was taken and analyzed by cutting and exposing a cross section of substrate immediately prior to analysis. The results are in Figures 4-14(a-c) and Tables 4-8, 4-9, and 4-10. Intensity changes provide

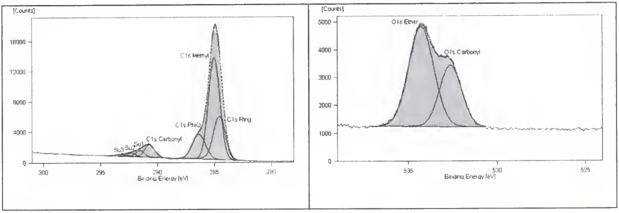

(a) Raw XPS data from fresh sample

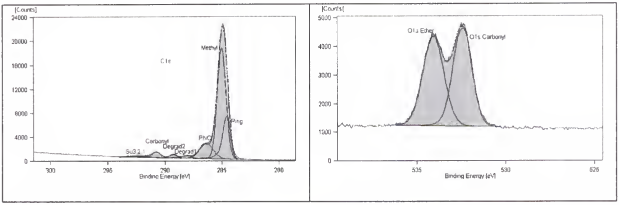

(b) Raw XPS data from clear sample

Figure 4-14(a-c). XPS analysis raw count data for bulk, masked, and etched areas.

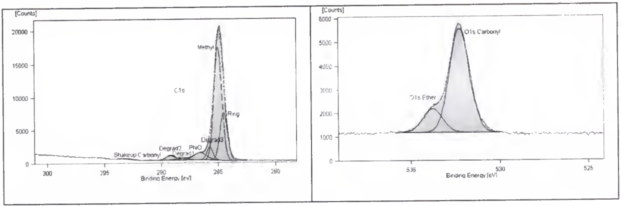

(c) Raw XPS data from etched sample

Figure 4.14(continued)

Table 4-8. XPS peak distribution data analysis from fresh sample in Figure 4-14(a)

Atom	BE (eV)	Fwhm	Area %
C_{1s} (Ring)	284.5	1.23	24
C_{1s} (Methyl)	285.0	1.18	55
C_{1s} (PhiO)	286.4	1.36	15
C_{1s} (Carbonyl)	290.7	1.05	6
C_{1s} (Su1)	291.5	0.86	
C_{1s} (Su2)	292.3	0.89	
C_{1s} (Su3)	293.2	1.22	
O_{1s} (Carbonyl)	532.6	1.45	35
O_{1s} (Ether)	534.3	1.66	65
Si_{2p}	102.5	1.57	

Table 4-9. XPS peak distribution data analysis from clear sample Figure 4-14(b)

Atom	BE (eV)	Fwhm	Area %
C_{1s} (Ring)	284.5	0.78	22
C_{1s} (Methyl)	285.0	0.89	60
C_{1s} (PhiO)	286.3	1.40	13
C_{1s} (Carbonyl)	290.8	0.85	3
C_{1s} (Degrad1)	288.0	0.97	2
C_{1s} (Degrad2)	289.2	0.72	2
C_{1s} (Su1)	291.5	0.66	
C_{1s} (Su2)	292.3	1.92	
C_{1s} (Su3)	292.6	1.90	
O_{1s} (Carbonyl)	532.4	1.26	50
O_{1s} (Ether)	534.1	1.40	50
Si_{2p}	102.3	1.22	

Table 4-10. XPS peak distribution data analysis from etched sample Figure 4-14(c)

Atom	BE (eV)	Fwhm	Area %
C_{1s} (Ring)	284.5	0.77	24
C_{1s} (Methyl)	285.0	0.81	59
C_{1s} (PhiO)	286.6	1.33	7
C_{1s} (Carbonyl)	291.1	0.45	0
C_{1s} (Degrad1)	288.0	1.21	2
C_{1s} (Degrad2)	289.2	0.73	3
C_{1s} (Degrad3)	295.7	0.63	5
O_{1s} (Carbonyl)	532.2	1.33	82
O_{1s} (Ether)	533.8	1.31	18
Si_{2p}	102.2	1.29	

valuable information about the molecular changes which occur in the case of a surface treatment as in Figure 4-14(c). The fresh and clear samples (Figures 4-14(a) and 4-14(b)) provide information about the unetched surface and act as a benchmark data set to compare the etched sample with. The most obvious changes between the etched and unetched samples occur in the oxygen bonding of the ether groupings. There is also a dramatic increase in the intensity from the cabonyl structure. Ether group destruction is likely due to effect of the plasma breaking up the molecular chain of the polycarbonate by the mechanical energy from ion bombardment. Carbonyl group formation is likely enabled by the high amount of reactive oxygen ions generated in the plasma environment and interacting with the high energy surface structures created from mechanical degradation.

Comparison of these results can be made to the model for A-bisphenol polycarbonate provided in section 3.4.5. This comparison shows some slight differences between the bulk model and fresh sample analysis in Table 4-8. The most apparent difference between the two sets of data is evident in the ring and methyl peaks which are not consistent. This may be due to a slightly modified molecular structure than A-Bisphenol.

This does not present any problems for our purposes as the standard for comparison can be made to the fresh sample in Table 4-8. The raw data graphs showing silicon peaks which appear to occur around 102eV are not shown in the Figures in 4-14. This silicon is most likely due to the silicon wafer being used as an etching mask in the preparation of these samples.

4.2.1.6 Fourier transform infrared spectrometry (FTIR)

As a compliment to XPS analysis, FTIR also provides chemical bond/structure information. This analysis is quite simple and quick to perform. FTIR analysis was performed on one etched and one unetched sample. Figure 4-15 presents FTIR surface analysis results.

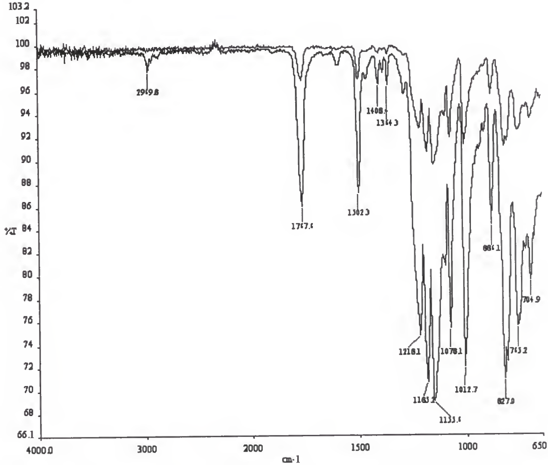

Figure 4-15. FTIR spectrum analysis of etched and unetched polycarbonate surface.

The lower scan is of the unetched PC substrate surface while the upper scan was taken of the etched surface (Table 4-5; condition R - 5000sec.,80W,80mtorr). The most impressive result from this analysis is the absence of the methyl group after surface treatment. Methyl (CH_3) groups are characterized by absorption most noticeable at 2962 cm^{-1} and 2872 cm^{-1} [46]. There is also a noticeable reduction in spectral absorption around 1600 cm^{-1}. This is most likely due to attack on the benzene ring structure and the C=C bonding which exhibits an absorption peak at 1600 cm^{-1}. Attack of the methyl groups and the benzene ring are possible when energized oxygen ions are used for long etching time as was the case for this sample. Long etching time was used for this FTIR analysis due to the relative lack of sensitivity when compared to other techniques such as XPS. The comparison of results between this analysis and those obtained using XPS must take the difference in etching time in to careful consideration.

4.2.2 Adhesion Characterization

Adhesion testing using the cross hatch scratch test detailed in section 3.5 was performed on all samples. The scratch test results are presented in Table 4-11. Figure 4-16 presents main effects analysis for the three factors evaluated.

Table 4-11. Scratch test adhesion results for blanket oxygen treatment.

ID	Etch Time (sec) /Power (watts) /Pressure (mtorr)	ISO 2409 Adhesion Scratch Test Results
A	160 /40 /40	2
B	160 /40 /160	2.5
C	160 /160 /40	1.5
D	160 /160 /160	1
E	660 /40 /40	1.5
F	660 /40 /160	2
G	660 /160 /40	1
H	660 /160 /160	2.5
I	300 /80 /80	2.5
J	0 (control)	4

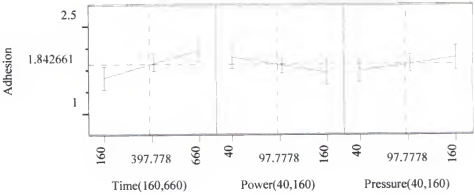

Figure 4-16. Factor midpoint scratch test results main effects analysis.

Scratch test main effects trending shows adhesion to be maximized (lower value = better adhesion) by moving toward higher power, lower pressure, and shorter etch times. Figure 4-17 shows the case where the plasma conditions are considered to be the most gentle which occurs at high pressures and low powers.

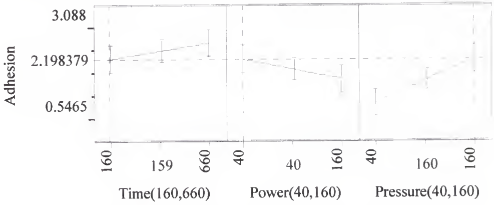

Figure 4-17. Scratch test results main effects analysis – gentle plasma conditions.

For gentle plasma exposure, pressure seems to be a highly significant factor when unagressive plasma conditions are considered. Low pressures generally create an environment in which there becomes a high ion bombardment component to the etch. This trend is shown by the high negative slope of the pressure curve. Alternately, consideration of what would be deemed the most aggressive conditions (low pressure, high power) are shown in Figure 4-18.

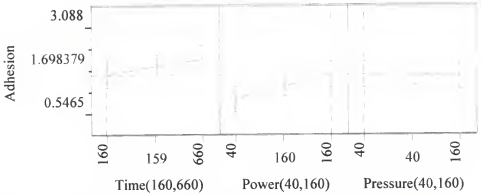

Figure 4-18. Scratch test results main effects analysis – aggressive conditions

Figure 4-19 shows that the optimal conditions to realize the best adhesion occurring at low etch time, low power, and low pressure.

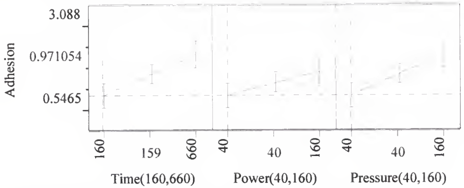

Figure 4-19. Scratch test results main effects analysis – optimal conditions

These results do not correlate very well to the behavior expected based on AFM and contact angle measurement results. At the outset of this work, it was expected that a very strong correlation would be found between high surface roughness and better adhesion. It was originally thought that high surface roughening would provide more surface area for substrate-thin film interaction and physisorption. Maximum roughness was found to occur for Sample H (660 sec, 160 watt, 160 mtorr). Sample H also showed the lowest contact angle indicating maximum free surface energy. Those conditions to which sample H were exposed are not in alignment with those found to exhibit the best adhesion as shown in Figure 4-17.

4.3 Discussion

4.3.1 Structural Morphology

4.3.1.1 Surface structure alteration and measurements

AFM data shows us that surface roughness and surface area is being created during the etching process. This roughness leads to increased surface area. The origin of roughness evolution are not well understood and not the subject of this study. Some level of insight in to the source of roughness evolution can be gained by looking at the dense pattern vs. isolated pattern roughness measurement data. The fact that there is a difference between the two areas leads us to believe that the masking during polymer etching may have a significant effect on the etching fundamentals and in the creation of surface roughness through inorganic small particle material micromasking.

AFM results show striking differences in surface roughness within the process space evaluated between 160 to 660 seconds etch time, 40 to 160 watts power, and 40 to 160 mtorr pressure. The results can be seen by visual investigation of the AFM micrographs generated and through roughness analysis of the data. The maximum roughness occurred at maximum time, power level, and pressure (Sample H). Within the process space evaluated, this tells us that higher plasma density which are the result of these conditions are more effective in the creation of roughened surfaces. This finding fails to take in to account the effect of total etch depth. Further investigation showed similar results which further strengthen the finding of maximum roughness evolution for high power and high pressure plasma conditions. The affinity for roughness evolution under these conditions might be explained by considering the plasma situation and environment created under these conditions at the substrate surface. The combination of both high pressure and high power provides a situation where an excessive amount of gas is readily ionized under the high power filed. This provides many active species. At the same time, a high pressure environment decreases the ion impact energy at the substrate surface. In short, there are many active species possessing relatively low surface impact energy. In this situation, there is more opportunity for chemical etching and species surface migration which may lead to clusters of etching activity. This process may provide a better opportunity for island formation which can ultimately result in roughness evolution.

Contact angle measurements were used as a means to assess the level of surface free energy created by the various plasma conditions. Again, it was found that Sample G (maximum etch time, power, and pressure) produced the surface with the highest measured level of free energy as determined by the minimal contact wetting angle. This measurement technique is important because it provides a real measurement of surface free energy which can be used to draw conclusions about the propensity of the treated surface to attract and adhere another thin film or surface. When treated in a plasma environment, the polymer surface is roughened as well as structurally changed on a molecular and atomic level. The mechanisms of chemical and mechanical attack create molecular fragments with unbound groups and atoms. These active regions may become unstable and contribute to the overall free energy of the system at the surface. This free energy is a net attractive force due to unstable atoms or molecules which become more polar due to segmentation. The availability to excess free energy is what is important in the phenomenon of physisorption and the ability of a surface to attract and adhere to a second applied surface. Because water is a highly polar molecule, it is used here in the measurement and assessment of the surface. The very low contact angle of the high power and high pressure condition is likely due to the creation of a surface with excess oxygen bond formation from an environment in which many active oxygen species are generated and available for forming bonds with active regions/atoms on the surface. Oxygen bonding has the ability to create highly polar molecules leading to excess free surface energy and low contact angles.

Analysis using XPS shows that the roughness evolution observed in AFM analysis results may be due to micromasking from particles or atoms dislocated from the mask material. The presence of silicon in the analysis suggests that the inorganic masking material is being attacked by the plasma environment, dislodged, and deposited on the polymer etch surface. This is likely for the clear and the etched samples as a silicon mask material was used on this wafer. The presence of a silicon peak in the fresh sample is puzzling. This may be due to contamination of the cutting mechanism or blade used to perform the cut to expose the interior surface of the polycarbonate substrate.

4.3.1.2 Chemical modification

Both XPS and FTIR analytical analysis data indicate that the PC structure is significantly altered by plasma etch treatment. Attack appears to occur readily for the methyl and carbonyl groups. Benzene ring attack is also seen – but only for longer etch times. All data indicates that the breaking of bonds is occurring due to plasma exposure. This leads to dangling bonds which is believed to be a significant source of excess surface energy.

Analysis of the XPS data provides additional insight in to the chemical affects of the plasma environment. The fresh specimen exhibited very nearly the expected spectrum of an aromatic polycarbonate as presented in Section 3.4.5, along with a small amount of Si (probably SiO_2). The polycarbonate is characterized by a C peak at 290 eV binding energy with a tail to higher energies (shakeup peaks from aromaticity). Oxygen peaks are in the expected ratio of 2:1 for in-chain:carbonyl.

The clear area had characteristics of aromatic polycarbonate, silica, and some other compounds. Specifically, the polycarbonate C peak was reduced in size and a peak at slightly lower binding energy appeared. This may be an unterminated chain, i.e. R-O-C-O-. Also, the aromaticity may be reduced. The oxygen peak is changed significantly also, with a ratio of 1:1 for in-chain:carbonyl oxygens.

The etched area was essentially an extension of the clear area. Now, essentially all polycarbonate C is gone, while a little aromatic character remains. Oxygen peaks are again in a 1:1 ratio. Lastly, the Si peak is now twice as high as previously for the clear area.

The information gained through XPS analysis provides additional information to understand the typical mode of attack of the polycarbonate structure by a standard plasma condition. The plasma conditions chosen for samples analyzed was the center point condition for the matrix experiment (300sec, 80watt, 80mtorr). The information obtained validates the theory of free surface creation through both processes of dangling bond formation and oxygenation.

4.3.2 Adhesion Characterization

Scratch testing of substrates treated under various plasma conditions and coated with a fluoropolymer thin film were evaluated. This test method is quite subjective in nature, but results obtained in this work do show distinct differences which were categorized according to standard test methods. The best adhesion resulted from plasma conditions of minimum time (160sec), minimum power (40mtorr), and minimum pressure (40mtorr). At the outset of this work it was thought that physical surface roughening would lead to better adhesion. These test results proved this not to be true. Those conditions which produced the greatest level of surface roughness and the lowest contact angle did not prove to be effective in promoting adhesion. A general trend is present in the data which suggests that longer treatments on the order of 11 minutes are less effective than those around 2-5 minutes. More importantly, the factor of pressure was a significant factor in the determination of adhesion strength – especially for longer etch times. Low pressure conditions were very effective in producing the best adhesion performance. The conditions for sample G (660sec, 160 watt, 40 mtorr) which resulted in the smoothest surface from AFM analysis also produced the best adhesion results. These results are not as expected. The capacity for the low pressure condition to improve adhesion may be due to the high degree of mechanical energy through ion bombardment. Low pressures create a plasma environment and a sheath region with a high mean free path between species. This situation enables ions to possess more energy due to fewer inelastic collisions. The overall energy of ion bombardment at the substrate surface is much greater which may lead to more effective physical degradation of the polymer with less chemically reactive species for recombination. It is possible that deeper penetration in to the surface is achieved and that this is more effective in bonding with a solution cast thin film.

The analytical results can be used to determine trends and relationships between adhesion strength, RMS surface roughness, surface area, contact angle, and etch depth. Figure 4-20 is a multivariate scatterplot matrix with correlation factors shown in Table 4-10. It shows that the factor with the strongest influence on adhesion is surface area with a correlation factor of .656. Second order predictor was RMS roughness with a .503 correlation factor. Surprisingly, Contact angle has the smallest correlation with a factor of .395. Overall, the absolute correlation strength of any one factor is unimpressive. The emergence of surface area as the most significant predictor of adhesion may be the result of a strong relationship between this factor and surface area. The scatter plot provides a

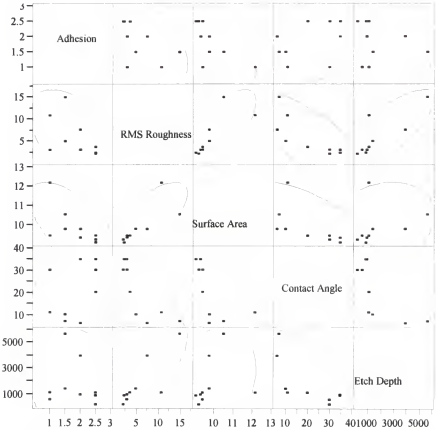

Figure 4-20. Multivariate scatterplot of adhesion test analytical result relationships.

Table 4-10. Multivariate correlation factors from adhesion factor scatterplot analysis.

	Adhesion	RMS Roughness	Surface Area	Contact Angle	Etch Depth
Adhesion	1.0000	-0.5028	-0.6563	0.3954	-0.1717
RMS Roughness	-0.5028	1.0000	0.7591	-0.7814	0.8173
Surface Area	-0.6563	0.7591	1.0000	-0.6058	0.2755
Contact Angle	0.3954	-0.7814	-0.6058	1.0000	-0.7014
Etch Depth	-0.1717	0.8173	0.2755	-0.7014	1.0000

summary snapshot of all the factors that are thought to be potential contributors to adhesion strength.

4.4 Summary

Blanket oxygen plasma etching of plastic substrates to enable fluoropolymer thin film adhesion was evaluated. Samples were prepared and analyzed through various analytical means such as profilometry, AFM, contact angle, XPS, FTIR, and cross hatch scratch test analyses to provide a fundamental understanding of the mechanisms contributing to the modification of polymer surfaces for adhesion enhancement.

Cross hatch scratch adhesion testing of various experimental samples provided a range of results and levels of adhesion among treated samples. All levels of treatment were quite effective when compared to the extremely poor adhesion of the untreated sample. Test results showed that one of the most potentially significant factors in promoting good adhesion lies in the plasma chamber pressure. The low pressure condition of 40 mtorr proved to be most effective. This condition was also that which produced the smoothest etched surface from AFM analysis and the lowest contact angle measurements which was a very surprising finding. In a comprehensive comparison between the various categories of analytical results and adhesion, the most significant indicator of adhesion strength was that of surface area. RMS roughness proved to be a secondary indicator to that of surface area. Not as effective as RMS roughness was the measurement of surface water contact angle. Finally, the etch depth proved to have almost no correlation to adhesion.

Chemical bond analysis using FTIR and XPS show that the surface molecules are quite effectively broken down and altered with significant dangling bonds being created primarily through breakdown of the ether, methyl, and aromatic ring groups. Evidence suggesting the existence of surface oxidation in the growth of carbonyl group formation was also seen.

Adhesion improvement via surface area increase was shown to be highly effective. Higher surface area trends were shown to result for longer etch times independent of power and pressure. For a set etch time and low power (40 Watts), lower pressure (40 mtorr) was more effective in the creation of high surface areas. An inverse relationship occurred at high power (160 Watt) which resulted in maximum surface area at high pressure (160 mtorr). The highest values of surface area were produced under condition of maximum time (660sec), maximum power (160 Watt), and maximum pressure (160mtorr). This condition did not prove to be the best adhesion condition. AFM micrographs show this condition to be abnormally rough by a factor between two and five times when compared to the other comparable samples in the core matrix experiment. This anomaly leads to the belief that there is another factor such as pressure which may be very influential in the conditioning of a surface for high adhesion.

These results show that there is a limited yet real ability to affect the adhesion between polycarbonate substrate and fluoropolymer thin film using blanket oxygen plasma etching. Since the plasma etch process is limited to the factor ranges evaluated in the experimental matrix as a result of chamber design and thermal limitations, it is safe to say that the results are roughly indicative of the maximum enhancement available via this technique. Qualitative scratch testing results in addition to a broad range of surface analysis techniques were quite effective in providing a better understanding of the ability to alter polymer surface properties in the enhancement of adhesion. The use of scratch testing provided valuable but limited results due to the subjective nature of pattern rating.

The factors contributing to the enhancement of a polymer surface for adhesion purposes have been studied. Various surface analysis methods indicate that adhesion is a stronger function of surface area than any other factor. An effective treatment method consists of one in which produced maximum total surface area. There exist limitations to this method of blanket plasma surface treatment as shown by the scratch test results in which no single sample evaluated produced the ultimate level of adhesion as measured by the ISO 2409 test standard.

CHAPTER 5
RIE SURFACE MICROFEATURE FORMATION

Chapter 4 showed that there exist limitations of blanket plasma treatment in the attempt to improve adhesion between polymer and fluoropolymer surfaces. Thus, the need for the development of an alternative and more advanced technique is critical to the further advancement of advanced fluoropolymer waveguide/thin film coating technology. The use of microstructures formed on the surface of the substrate presented in this chapter is a novel solution to the adhesion problem between a hydrocarbon polymer substrate and solution cast fluoropolymer thin films. In this approach, microstructural anchors are formed using RIE and plasma etching with the assistance of thin film metallization and photolithography. These microfeatures formed in the substrate act as a mechanical grip on the fluoropolymer thin film to prevent macroscale delamination.

5.1 Background

The interest in fabricating surface microfeatures as a means to improve adhesion originated from the belief that, all other factors being equal, the adhesion strength should have high correlation to the surface area density on the substrate. This should be the case because the primary attraction mechanism between the fluoropolymer thin film and the hydrocarbon polymer surface is by increasing the surface free energy. Greater surface area provides greater exposure to available free energy to increase surface van der Waals bond forces. The effect of surface area on adhesion was found to be an extremely important and highly effective factor from the work in the previous chapter. The strong correlation between measured surface area and adhesion level in Chapter 4 presents a strong experimental basis for predicting the success of microfeatures in adhesion enhancement.

In the course of this work it was conceived that, in addition to improved surface area interaction via microfeatures, it was possible to use these structures also to mechanically lock the two surfaces together by fabricating the features in certain geometrical "upside-down pyramid shaped" structures as shown in Figure 5-1. Fabrication of these geometries on the surface of polymer substrates may be accomplished by strategic adjustments to the process parameters during the etch.

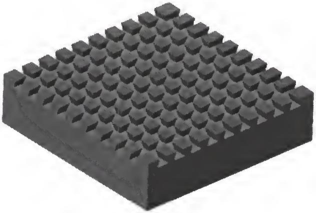

(a) microfeature covered substrate surface (international patent # WO 03/078304)

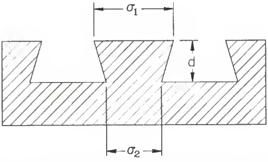

(b) microfeature cross section profile (international patent # WO 03/078304)

Figure 5-1(a,b) Microfeature covered substrate surface(a) and cross section profile(b) [47].

It was proposed that the effectiveness of these structures could be maximized by forming them over the entire substrate surface prior to fluoropolymer thin film casting. The fluoropolymer, which is cast in solution form by the spin coating technique, would readily flow and wet fully to the microfeature surfaces assisted by the high wetting to the high energy substrate surface resulting form the plasma processing. The baking procedure (following casting) would solidify the fluoropolymer thin film to form a locking interface resulting in a high strength mechanical bond between the surfaces.

Initial work in the evaluation of this formation was focused on the effort to determine optimal metrics as well as process capability for such critical attributes as feature cross section profile, coverage density, and feature aspect ratio.

Early work and consideration of process capabilities/limitations resulted in a preference for features on the order of 5-10μm^2 which were found to be the minimum sized features with satisfactory structural integrity. One of the limiting factors governing the minimum feature size rested with the resolution capability of broadband exposure contact mode patterning. Under these conditions, photolithography becomes a challenge for sub 4μm features due primarily to the variability in substrate flatness and the capability of the contact exposure equipment being used. Further information concerning the contact exposure photolithography procedure used for this work is contained in Appendix B. In addition to limitations based on patterning difficulty, smaller feature formations with aspect ratios greater than 4:1 were prone to breaking at the base before, during, and after subsequent thin film casting. These features were much too fragile and would likely not hold up under environmental test conditions even if they proved to withstand the mechanical forces from spin coating.

For these experimental samples requiring a mask level, a silica glass chrome patterned photolithography mask such as that depicted in Figure 5-2 was used to pattern the features on the substrate surface using a Karl Suss MA-6 manual alignment vacuum contact exposure system. The mask features were chosen to be small squares arranged in an ordered matrix. This pattern was chosen to provide surface area maximization with linear pitch distance in any direction 200% of chrome mask pattern length. The size of the features was determined by consideration of the limits governed by the minimum resolution of the photolithography process and the attempt to maximize surface area (<10μm feature size with 20μm pitch). Using these guidelines, 5x5μm, and 10x10μm square features were chosen for evaluation. Using these mask pattern geometries, the etching process was chosen so as to produce features with target aspect ratios between 1:1 and 1:3 based on the minimum mechanical feature structure integrity limitations discussed previously. These feature size ranges were chosen to explore the entire set of

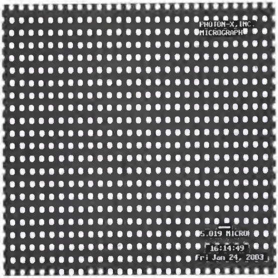

Figure 5-2. Mask pattern for microfeature evaluation experiment – optical micrograph.

available and realistic process conditions. The end goal was to produce the widest range of surface area creation without compromising mechanical strength/structure integrity of the microfeatures.

The plasma conditions were fixed for these evaluations due to the strong belief that additional factors in the experiment would lead to confounding results. Etching conditions for this evaluation were chosen to be those consistent with high surface area creation as determined in the work in Chapter 4: 160 watt, 40 mtorr, 35°C wall/cathode temp, 100 sccm O_2. These condition were chosen based on the results in section 4.2.2 Table 4-9 which proved most effective in surface activation for long etch time where power, and pressure were considered to be the relevant factors.

An initial screening experiment was performed to evaluate the full range of various sizes and post etch feature aspect ratios as outlined in the preceding paragraphs. In addition, this preliminary information was important to understand etch rates, etch feature profiles, and to obtain preliminary information and adhesion results. Table 5-1 shows the screening factorial experiment matrix and conditions evaluated:

Table 5-1. Screening experiment matrix for microfeature evaluation.

Substrate ID	Feature mask pattern size (µm)	Etch Depth (µm)	Aspect Ratio
A	5X5	7	1.4
B	5X5	15	3
C	10X10	7	.7
D	10X10	15	1.5

100mm polycarbonate substrates were prepared, fabricated, and analyzed using the conditions contained in Table 5-1 and the fabrication techniques of photolithography and plasma etching as described in Section 3.2.2.2. Plasma conditions for all samples were 160 watts and 40 mtorr. The target etch depth was achieved using calculated etch rates from Section 4.2.1.1.

5.2 Results

5.2.1 Structural Characterization

The analytical analysis techniques of SEM microscopy, profilometry, and cross hatch scratch test adhesion testing were utilized to characterize the process and the performance of the system. The methods and conditions used to generate SEM micrographs are presented in Section 3.4.1. The non-conductive nature of these samples required the sputter deposition of 100 angstroms Au/Pd alloy to prevent charging of the sample under electron SEM electron beam bombardment. The methods to obtain the following profilometry data are in section 3.4.3. The techniques used in adhesion testing are in section 3.5.

5.2.1.1 SEM analysis

The screening experiment from Table 5-1 produced the micrographs in Figure 5-3. These images were obtained using scanning electron microscopy: All images were captured at 3,700 times magnification with an electron beam energy of 5kV. Samples were mounted on a stainless steel mounting block using conductive tape to promote charge dissipation. The maximum working distance allowed by the system was used to provide adequate depth of field to allow full focusing of the three dimensional microfeatures. Samples were analyzed at a 45 degree stage tilt. Figure 5-3a shows the post processed surface of sample A. The surface is covered with a high density of structurally stable looking features. The features in Figure 5-3d show evidence of maximal structural integrity. These conditions appear to provide the maximum surface area while still maintaining structural integrity. The features from sample B in Figure 5-3b appear very stable with an extremely high level of bottom etch surface roughness but lacking in surface area creation. Sample C in Figure 5-3c looks structurally unsound and

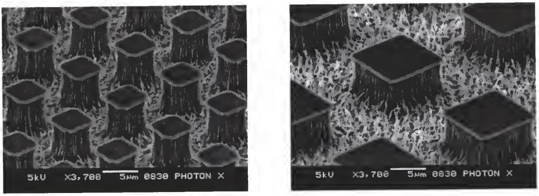

(a) 5µm x 5µm x 7µm

(b) 10µm x 10µm x 7µm

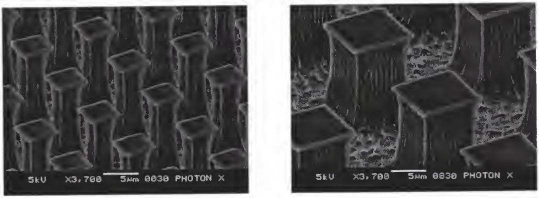

(c) 5µm x 5µm x 15µm

(d) 10µm x 10µm x 15µm

Figure 5-3(a-d). SEM micrographs of etched microstructures; (a) 5µm x 5µm x 7µm (length x width x height), (b) 10µm x 10µm x 7µm, (c) 5µm x 5µm x 15µm, (d) 10µm x 10µm x 15µm.

highly prone to breaking. Sample D in Figure 5-3d is very stable looking without compromise in total surface area generation due to the deep etching.

The SEM micrographs shown here were taken directly after the plasma etch process and prior to removal of the aluminum etch mask. This was done to help with charge dissipation and to provide some understanding of the degree of undercut beneath the metal masking layer. This information is useful in the determination of the degree of anisotropy of the plasma etching conditions. This understanding is useful to determine the appropriate adjustments to the plasma conditions to achieve the desired profile.

5.2.1.2 Profilometry analysis and etch roughness evolution

The micrographs in the previous section show an extremely high degree of etch surface roughness. We have seen the characterization of the roughness and related surface area creation in Chapter 4 using AFM analysis. For this approach, where very deep etching on the order of 5-15 microns is the case, the roughness level is too severe for measurement by AFM technique. Profilometry can be used to study the phenomenon of surface roughness for deep etched structures where the roughness is on the order of 50nm or greater. Below this threshold, AFM is the preferred technique. Although the structures being fabricated have etch depths comparable to some of the cases evaluated for surface treatment as discussed in Chapter 4, the etch surface roughness was significantly different for these patterned surfaces. Roughness was much more pronounced for these patterned substrates (on the order of >50nm RMS) when compared to those that were unpatterned. For these surfaces, profilometry was used due to the capability to measure high level surface roughness with better accuracy.

The effect of mask patterning on polymer surface etch roughness evolution is not fully well understood. There are two plausible explanations. The first contends that the roughness is believed to be caused by the interference by dislocated mask material or from field interference of the mask step height on the plasma field. This does not explain the roughness evolution for unpatterned wafers which also is shown to occur unless contributions from the chamber sidewall or wafer shadow ring are considered. The second possible explanation proposes that the roughness is due to an accumulation of structures in the polycarbonate molecule which are not decomposed by the plasma environment such as the aromatic ring structure. These groups form clusters of unetchable matter.

To further understand this phenomenon, a matrix experiment was performed to study variation in pattern pitch size and etch depth and their effect on bottom etch surface roughness. For this experiment, three levels of pattern pitch were investigated (10, 5,000, and 20,000μm) along with four levels of etch depth (5, 20, 40, and 60μm) as outlined in Table 5-2.

Table 5-2. Pattern size vs. etch roughness evolution.

Sample	Etch Depth (μm)	Pattern Pitch (μm)
A	5	10
B	5	5000
C	5	20000
D	20	10
E	20	5000
F	20	20000
G	40	10
H	40	5000
I	40	20000
J	60	10
K	60	5000
L	60	20000

Figure 5-4 shows the results of RMS roughness analysis obtained using profilometry measurements on the samples processed according to Table 5-2. These results show the level of surface roughness to be highly dependent on the etch depth. This is not surprising since the results in Chapter 4 showed the same dependency. The more interesting part of the data indicate that the roughness is also highly dependent on the

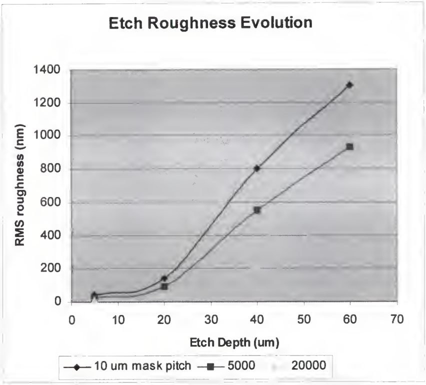

Figure 5-4. Mask pattern Size vs. etch roughness.

pattern pitch size. Smaller pitched features (10µm) exhibited a greater roughness level which decreased somewhat linearly with increasing feature pitch size. Furthermore, this dependency is significant for features etched to depths greater than 20µm or more. Smaller pitch features were especially prone to higher levels of surface roughening most likely due to ion/neutral imbalances which come in to play with very high aspect ratio features.

Average peak – valley measurement are also important considerations for evaluation. These values were measured using the same techniques as RMS roughness and are presented in Figure 5-5. As in the case of roughness, both smaller pitch size and higher etch depth caused larger peak-valley measurements.

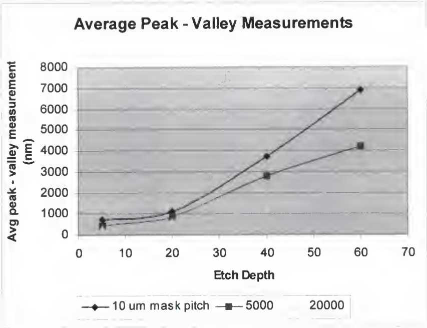

Figure 5-5. Average peak – valley measurement

Etch roughness dependency on pattern pitch is most probably due to dislocated fragments of inorganic mask materials which end up landing on the polymer etching surface and result in micromasking. It is difficult to estimate the effect of this roughness on adhesion. It would seem that this roughness creates significant surface area on the bottom surface of the etched areas. It is likely that the roughness created is not structurally rigid, but rather quite soft and easily washed, blown away. In this case, there is no added affect from this roughness/surface area on adhesion.

5.2.1.3 XPS analysis

In addition to the samples for blanket oxygen etch evaluation in 4.2.1.4, one additional sample was analyzed consisting of a substrate masked by a photolithography pattern with a 20,000µm space (open area for etching) and 50,000µm line (masked area) similar to those samples from Table 5-2. The etch depth for this sample was on the order of 60µm. The deep etching was used to provide an extreme case of roughness as an example for analysis. These samples were chosen for analysis based on restrictions to the lateral resolution capabilities of the XPS analysis. The masking material was photoresist patterned aluminum. The photoresist was fully removed during the etch procedure. XPS data obtained from the analysis is presented in Figure 5-6 and Table 5-3.

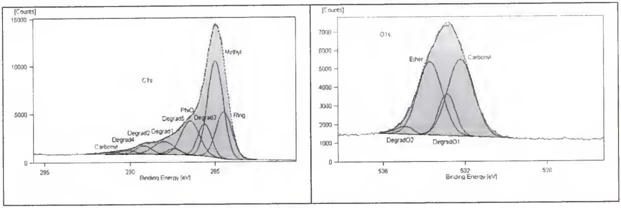

Figure 5-6. XPS analysis raw count data for tight pitch patterned sample etched to 60μm.

Table 5-3. XPS peak distribution data for tight pitch patterned sample etched to 60μm .

Atom	BE (eV)	Fwhm	Area %
C_{1s} (Ring)	284.5	1.11	19
C_{1s} (Methyl)	285.0	1.07	39
C_{1s} (PhiO)	286.5	1.27	16
C_{1s} (Carbonyl)	290.8	1.28	1
C_{1s} (Degrad1)	288.0	1.49	7
C_{1s} (Degrad2)	289.2	1.09	3
C_{1s} (Degrad3)	285.6	0.97	11
C_{1s} (Degrad4)	290.2	1.11	2
C_{1s} (Degrad5)	287.4	0.96	2
O_{1s} (Carbonyl)	532.2	1.51	43
O_{1s} (Ether)	533.7	1.41	39
O_{1s} (DegradO1)	532.8	0.97	15
O_{1s} (DegradO2)	534.9	1.06	3

This XPS analysis data for this masked and deep etched sample is markedly different from the three samples in section 4.2.1.4. One of the most striking findings is that there is that there is found no silicon present in the spectrum as was the case in the previous clear and etched samples. The lack of silicon is expected due to the use of an aluminum masking material for this sample. Otherwise it looks like a polycarbonate that has lost some polycarbonate character, much like that clear and etched samples above.

5.2.2 Adhesion Characterization

Initial evaluations prior to full device fabrication and testing showed significant adhesion improvement for samples prepared with microfeatures when compared to those of untreated samples. These tests were based of thin film peel testing by taking a tweezer and attempting to peel back the fluoropolymer thin film from the substrates. In the case of the untreated sample, peeling occurred readily without much resistance. In the case of the microfeature treated substrates, a much different response was observed. In this case, peeling did not occur. The fluoropolymer thin film experienced breakage almost immediately upon receiving an applied pull force.

The next step in evaluation required the testing of adhesion performance for fully fabricated devices. Singulated device chips with full waveguide device fabrication from wafers treated according to substrate microfeature surfacing conditions in Table 5-1 sample D were prepared from the screening experiment. The decision to use sample D feature dimensions for full device testing in Chapter 6 was based on an attempt to both maximize surface area while completely assuring structural integrity. The decision not to use Sample A which provided more surface area was due to concern about the strength of the features. Since their strength was not well understood, the decision to use larger structures in sacrifice of some degree of surface area was made.

5.3 Discussion

5.3.1 Structural Characterization

The SEM micrographs in Figure 5-1 show the existence of 'T'-topping of the microfeatures. This is a phenomenon produced by plasma etching in which the top of the etched profile is wider than the remainder. This structure is desired for adhesion because these features act to mechanically hold the later cast thin film in place. This mechanical holding in place is conceptually a very effective method of creating and maintaining adhesion. The sidewall profile produced by the plasma etching conditions is difficult to measure and quantify as there exists curvature as seen in the micrographs from Figure 5-3. This curvature may be as effective in creating a physical hold as the inverse pyramid structure originally proposed at the outset of this work. Although further process development may be effective in producing a more highly undercut feature, the results obtained using the plasma etch conditions in the initial screening experiment (160 watt, 40 mtorr) appear to produce a satisfactory feature profile for further full device adhesion testing.

The aspect ratio range between 1:1 and 3:1 was qualitatively assessed using the micrographs in Figure 5-3. The desired combination of high mechanical strength of the features and maximum surface area generation was found to be acceptable within this range.

5.3.3 Etch Roughness Evolution

The bottom surface etching plane is affected by surface roughness as shown in Figure 5-3. As the mask pitch is decreased, the surface roughness increases as discovered through profilometry measurement analysis of fabricated samples of various pitch dimensions as seen in Figure 5-4. The understanding and modeling of this phenomenon is significant due to the strong relationship between surface morphology and adhesion – especially in the case of surface area. The fact that patterned samples are affected differently than those which were not patterned will present various considerations when evaluating the contributing factors for microfeature based adhesion enhancement.

This phenomenon is most likely the result of the mask material dislocation and micromasking or accumulation of local areas of highly etch resistant molecular groups from the polymer as discussed in section 4.3.1.1. This interference acts to alter the ion trajectory in the plasma. Agarwal et al. has reported similar findings in the etching of polyimide material [48]. Their work points to a theory presented by Drotar et al. in which "redistribution of the reactant gas flux is affected by local morphological features". This is consistent with the findings in this study. The source of the morphological features is still not fully understood.

5.4 Summary

The creation of 'T'-topped microfeatures on the surface of a hydrocarbon polymer substrate appears to be an effective method of creating and maintaining adhesion for a solution cast fluoropolymer thin film. Initial evaluation testing using the peel test method shows promising results when compared to untreated surfaces. Although attempts to create an sharply undercut feature seem to be not fully successful, the microfeatures produced with curvature to their sidewalls appear to be extremely effective as adhesion promoters. This is most likely due to both the increased surface area and the mechanical grip mechanism enabled by the concave sidewalls.

The phenomenon of etch roughness evolution and the relationship of the phenomenon to etching conditions has been reported previously by Agarwal et al [49]. The discovery in this work of a relationship also with mask patterning is a quite valuable finding. This pattern/pitch-dependent relationship seen in this study along with the XPS data in section 4.2.1.4 provides evidence to suggest that material dislocated from and inorganic etch mask may provide an important contribution to the evolution of surface morphology during polymer etching. This information presents new and important information in the attempt to understand the origins of polymer etch surface roughness evolution for unpatterned surfaces such as those in Chapter 4. The information obtained in this work suggest that there is reason for further investigation of effects from other sources of chamber hardware such as liners, chucks, shadow rings, and clamps.

CHAPTER 6
ENVIRONMENTAL DEVICE TESTING

The end goal of adhesion enhancement is to ensure long term performance and device reliability. Proof of reliability is a critical aspect in the ability to convince skeptics that polymer technology is capable of performing at the same level or better than conventionally accepted materials platforms such as silica and silicon. Proof of reliability is necessary out of the observation of many that the optical and mechanical characteristics of most polymers are not stable enough for operation in normal system operating environments, where temperature and humidity may vary. Thermal ageing of polymers commonly leads to oxidation and degradation which is evidenced by a yellowing of the material. This is a problem with many polymer systems but not all. Absorption of water in humid environments can interfere with signal propagation through the optical power absorption mechanism due to OH bonding[50]. New and specialized optical polymers such as the perfluorinated materials being evaluated in this work are much less severely affected by these ageing and absorption problems due to their unique properties. Additional effects on optical power absorption may be experienced under the appreciation of significant material stresses such as those created under thermal cycling conditions. In the effort to prove that polymer photonic devices can be made to withstand a wide range of environmental conditions, extensive environmental testing is required. The burden of proof rests in the generation of sufficient reliability data to combat the conventional industry prejudice that has plagued earlier generations of polymer optical materials and continues to act as a barrier to widespread industry acceptance.

6.1 Background

Environmental testing is used to simulate long term device field operating performance. For these devices, the ultimate test is to perform in-situ monitoring of optical power through the device. Since this testing is complex and can be affected by many intrinsic properties of the material which are not the focus of this work, device analysis under test conditions was focused on assessment of delamination of the fluoropolymer thin film stack from the plastic substrate.

Testing requirements vary between industries. Telecommunication industry specific specifications are most common and exist to test devices for environmental test failure. Telecordia GR-1312-CORE contains the "Generic Requirements for OFAs and Proprietary DWDM Systems Reliability Assurance Criteria". This is the relevant specification for integrated waveguide based telecommunications devices such as those for which this work has been performed. Table 6-1 details the requirements for GR-1312-CORE.

Table 6-1. Telecordia GR-1312-CORE reliability test standard for gain block and amplifier module [51].

Test Heading	Test Description	Test Condition	Sample Size	Failures Allowed
Fiber Integrity	Straight pull, side pull, flex, and twist		3	0
Mechanical	Vibration	5-50Hz, 0.1 oct./min, 1.5G, then 50-500Hz, 0.25 oct/min., 3G	3	0
	Mechanical Shock	200G, 1.33 msec pulse width	3	0
Environmental	Temperature Cycle	-40°C to 70°C, 100 cycles	3	0
	Damp Heat	85°C/85%RH, 1000 hrs.	3	0

These specifications were set up to measure device reliability appropriate for end application use in a communications system environment. For our purposes, the fiber integrity and mechanical tests are not directly affected by the substrate-thin film bond characteristics. The environmental tests of temperature cycling and damp heat are of critical importance. These tests are sufficient to evaluate the adhesion characteristics for the devices in this work.

The damp heat test is considered to be the most significant test in this case since water vapor is believed to be the primary cause for concern with respect to delamination. Shown in Figure 6-1, water vapor can attack by permeating through the substrate or by interacting with the exposed edge of the device since edges are highly shear force affected in the process of wafer saw die singulation. The adhesion between materials must be strong enough to prevent water vapor from attacking the interface between the fluoropolymer and substrate and causing delamination progression.

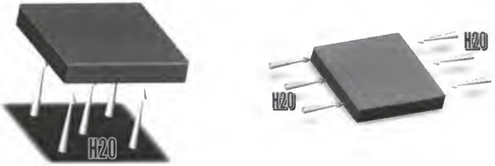

Figure 6-1. Water vapor attack on film-substrate interface.

Temperature cycling is also a very important test to evaluate adhesion properties due to the relatively high CTE values of polymer materials on the order of 60 ppm/°C. This is in sharp contrast to silica material with a very low CTE value on the order of 8 ppm/°C. Polymer systems experience significant expansion and contraction during thermal cycling. This thermally induced stress can have a detrimental effect on the adhesion properties for any physisorbed interface such as the structure being evaluated in this study. An appreciation of the material stresses imposed on the system under various testing conditions is important in the ability to fundamentally understanding the delamination issue. It is also paramount in understanding other failure modes such as cracking/crazing (shown in Figure 6-2) as well as stress absorption induced loss.

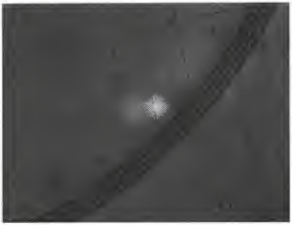

Figure 6-2. Network thin film cracking due to stress effects.

Stress effects can be modeled by considering the presence of a stress optic effect and process/operational stress (σ) as presented in equation 6.1 where *Ef* is the elastic

$$\sigma = \frac{Ef(CTEs - CTEf)(T_{process} - T_{ambient})}{1 - vf} \tag{6.1}$$

modulus of the film, *CTEs* is the thermal expansion coefficient of the substrate, *CTEf* is the thermal expansion coefficient of the film, *Tambient* is the ambient temperature, *Tprocess* is the process temperature, and *vf* is poisson's ratio. Higher CTE mismatch and more wide ranging thermal processes simply result in higher levels of stress. When CTE mismatch is present in as system, materials are expanding and contracting at different rates.

Delamination of thin film on substrate can be detected using optical microscope inspection. Careful inspection of samples will show thin film delamination as shown in the example in Figure 6-3. This device shows failure at the waveguide end face region characterized by an illuminated region being pointed to by the arrow. Failure is apparent due to optical interference effects which become prevalent in the region where detachment between the thin film and the substrate has occurred. The region of delamination has brighter appearance than the surrounding film. Another definitive characteristic is the presence of optical interference patterns/lines which can be seen within the delaminated thin film when not fully attached to the substrate.

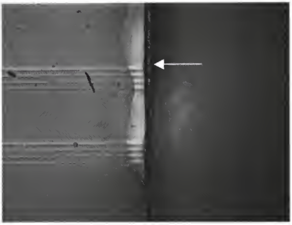

Figure 6-3. Optical micrograph showing an example of thin film de-lamination from the substrate.

Sample preparation, testing, and analysis of devices under environmental conditions of damp heat and temperature cycling was performed according to the procedures detailed in section 3.6. All samples were prepared through full device fabrication as detailed in section 3.2.2 with the appropriate surface conditioning (Sections 3.2.2.1 and 3.2.2.2) according to the experimental matrix shown in Table 6-2. Full device fabrication provided samples exposed to a realistic process history.

Table 6-2. Environmental testing experimental matrix.

ID	# Devices	Substrate	Surface Conditioning	Test
A	4	PC	None	Temperature Cycle
B	4	PC	None	Damp Heat
C	4	PC	O2 plasma 80W 80mtorr	Temperature Cycle
D	4	PC	O2 plasma 80W 80mtorr	Damp Heat
E	4	PC	etched 5x7µm microfeatures	Temperature Cycle
F	4	PC	etched 5x7µm microfeatures	Damp Heat
G	4	Zeonor	None	Temperature Cycle
H	4	Zeonor	None	Damp Heat
I	4	Zeonor	O2 plasma 80W 80mtorr	Temperature Cycle
J	4	Zeonor	O2 plasma 80W 80mtorr	Damp Heat
K	4	Zeonor	etched 5x7µm microfeatures	Temperature Cycle
L	4	Zeonor	etched 5x7µm microfeatures	Damp Heat

Following fabrication, substrates were sent to chip singulation where the individual devices with dimensions of approximately 2cm x 2cm were cut from their respective substrates. These devices were microtomed to provide smooth cut edges and end faces.

Testing was performed according to the guidelines in Table 6-1 for damp heat and temperature cycling to detect and cases of infant mortality due to physical delamination. Accelerated test methods of boiling/freezing water and pressure cooking were then utilized to predict device lifetime for the various treatment methods evaluated.

The boiling water/freezing water is an effective and generally accepted method of accelerated temperature cycling. Samples are simply immersed in boiling water for one minute, taken out, and then immersed in a bath of near-freezing water for one minute while periodically testing for delamination using a standard tape pull test.

Adhesion testing was performed using the destructive scratch test method to provide a final comparison between the methods presented in blanket oxygen treatment and microfeature formation. In this case, fully functional devices were fabricated as opposed to those tested in Chapter 4 which were only partially fabricated. Evaluation of fully fabricated devices is important to allow for many factors of thermal and chemical processing not previously considered or evaluated.

6.2 Results

Test results were obtained for both the standard real-time test conditions as well as the accelerated test methods for both environmental tests of temperature cycling and damp heat. Adhesion scratch tests results for untreated, blanket oxygen treated, and microfeature treated substrates were obtained and are presented.

6.2.1 Telecordia Temperature Cycling Test

Temperature cycling test results were generated through inspection of samples both prior to and directly following 100 cycles of -40°C/70°C. Samples from Table 6-2 were tested according to the procedure in section 3.6.1. Results were captured using optical inspection following testing and capture of optical micrographs using digital image capture and analysis software. Results are presented in Figure 6-4 for selected samples from each permutation of the experiment.

The results form this test are relatively unimpressive. There are no significant cases of delamination due to temperature cycling conditions. Sample A (untreated A-bisphenol polycarbonate substrate) was the only condition for which any sign of delamination occurred. This failure was not a result of the test method, but was already present prior to testing. The mechanical shear force from the wafer saw was great enough to cause delamination failure of the end face of the device even prior to testing. Upon optical inspection, all samples except for sample a are capable of passing the temperature cycling test.

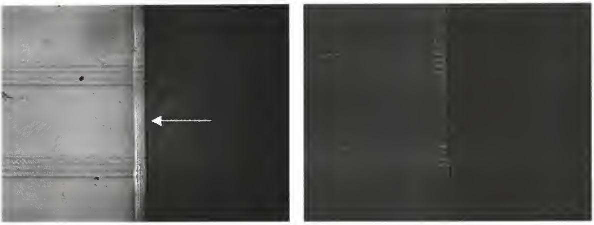

(a) PC no treatment - Pre

(a) PC no treatment – 100 cycles

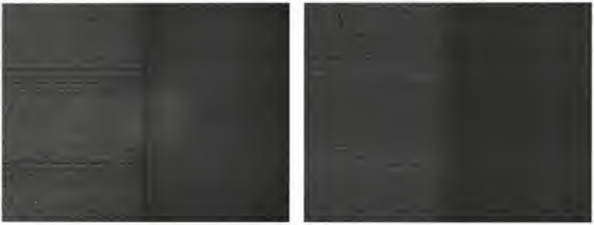

(b) PC blanket O_2 treatment - Pre

(b) PC blanket O_2 treatment – 100 cycles

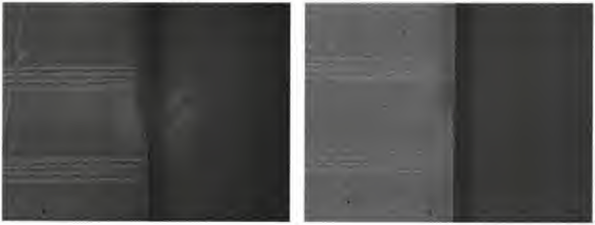

(c) PC microfeature treatment – Pre

(c) PC microfeature treatment – 100 cycles

Figure 6-4(a-f). Pre/post (100 cycles) temperature cycling test results.

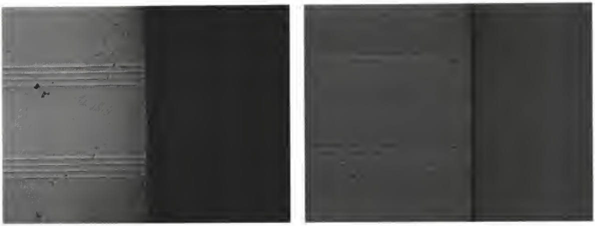

(d) ZNR no treatment - Pre

(d) ZNR no treatment – 100 cycles

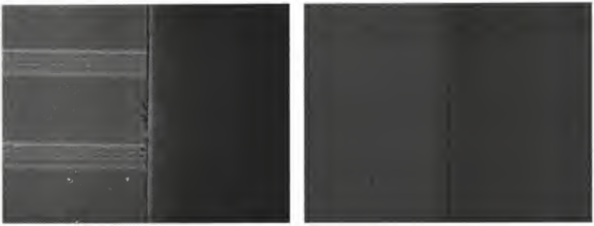

(e) ZNR blanket O_2 treatment - Pre

(e) ZNR blanket O_2 treatment – 100 cycles

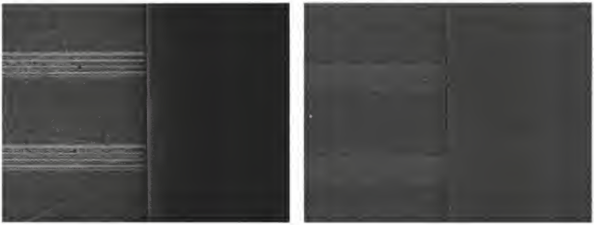

(f) ZNR microfeature treatment - Pre

(f) ZNR microfeature treatment – 100 cycle

Figure 6-4(continued)

6.2.2 Accelerated Temperature Cycling Test

One sample from each permutation (six samples in total) of the experiment from Table 6-2 were subjected to an accelerated temperature test utilizing boiling and freezing water as explained in section 3.6.2. Devices were tested to failure (delamination using the tape pull method). The results are contained in Table 6-3.

Table 6-3 Boiling/Freezing Water Immersion Test Results

Sample ID	# cycles to failure
A	22
C	56
E	>500 (did not experience de-lamination)
G	45
I	87
K	>500 (did not experience de-lamination)

The results first of all show evidence of an intrinsic property of the substrate which led to better across the board adhesion results for the Zeonor substrate (samples G-K) compared to the A-bisphenol polycarbonate substrates (samples A-E). This finding is of interest to this work because it proposes that there is another factor which can be used to improve adhesion outside of the realm of plasma treatment. Between samples A, C, and E, the untreated sample failed after only 22 cycles. The oxygen blanket treated sample held up for two times the duration which was expected from the results in Chapter 4. The performance of the microfeature treated sample was outstanding. Delamination did not occur after 500 cycles.

6.2.3 Damp Heat (85°C - 85%RH) Test

The 24 devices for this test according to Table 6-2 were placed in an environmental chamber on stainless steel racks. They were held and tested at 85°C/85 RH conditions for 1000 hours. Results are presented in Figure 6-5 for selected samples from each permutation of the experiment.

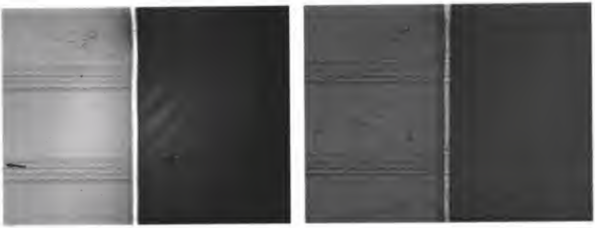

a) PC no treatment - Pre

a) PC no treatment – 1000 hrs

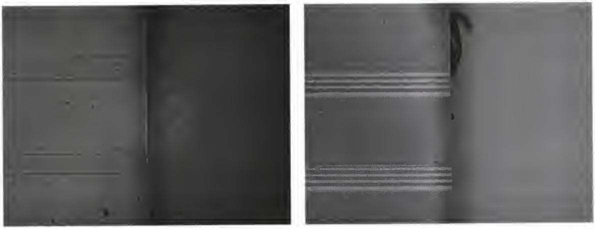

b) PC blanket O_2 treatment - Pre

b) PC blanket O_2 treatment – 1000 hrs

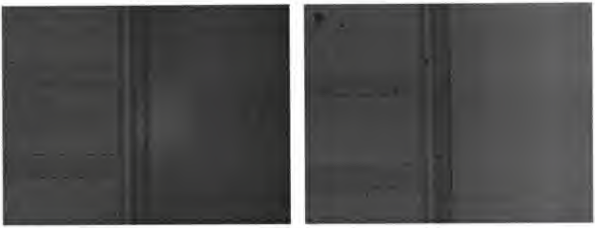

c) PC microfeature treatment - Pre

c) PC microfeature treatment – 1000 hrs

Figure 6-5(a-f). Pre/post (1000hrs) damp heat test results.

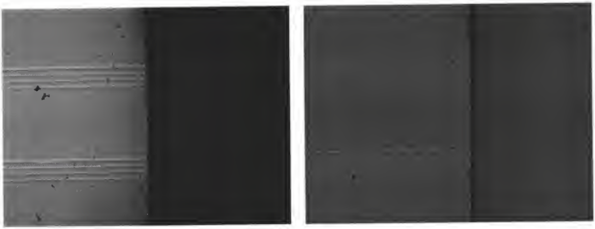

d) ZNR no treatment - Pre

d) ZNR no treatment – 1000 hrs

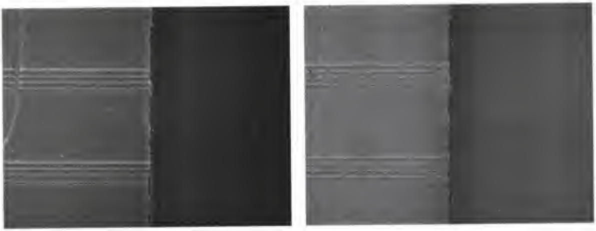

e) ZNR blanket O_2 treatment - Pre

e) ZNR blanket O_2 treatment – 1000hrs

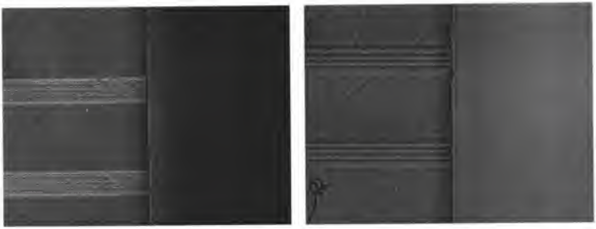

f) ZNR microfeature treatment - Pre

f) ZNR microfeature treatment – 1000 hrs

Figure 6-5(continued)

Similar to the case of temperature cycling, the damp heat test surprisingly showed only one case of delamination failure. This failure occurred for sample A – the untreated substrate surface condition.

6.2.4 Accelerated Damp Heat Test

An attempt to simulate the most extreme case of moisture exposure under high temperatures can be accomplished using a pressure pot and test procedure outlined in section 3.6.4. One sample from each permutation (six samples in total) of the experiment in Table 6-2 were subjected to the test. Devices were tested to failure (delamination using the tape pull method). The results are contained in Table 6-4.

Table 6-4. Pressure cooker accelerated damp heat test results.

Sample ID	**# cycles to failure**
A	6
C	23
E	>100 (did not experience delamination)
G	9
I	18
K	>100 (did not experience delamination)

When compared to the results from accelerated temperature cycling, the damp heat environment test showed very similar trends. The untreated sample failed first followed by the blanket oxygen treated sample. The microfeature treated substrate proved to be very robust and unable to fail even under the harsh conditions in this test.

6.2.5 Post Environmental Test Adhesion Scratch Testing

Scratch testing as performed as performed in Chapter 4 is the most effective method to assess the quality of the bond between the polycarbonate surface and the fluoropolymer thin film for fully fabricated optical devices. This destructive test requires some degree of subjective result evaluation, but with the aid of an optical microscope, the test method proved to be the most appropriate evaluation technique available. The cross hatch scratch test method was utilized to test devices from Table 6-2 upon environmental test completion. In this case, those sample chosen for test were taken from the set of devices which were subjected to damp heat testing as shown in section 6.2.3. The cross hatch scratch test as detailed in section 3.5 was performed on six samples representing three surface treatment levels (untreated, blanket oxygen treatment, and microfeature treatment) as well as two substrate types (A-Bisphenol polycarbonate and Zeonor). Optical micrographs are presented in Figures 6-6, 6-7. and 6-8 which show magnified areas of the scratch test area characteristic of the overall result. The micrographs shown in these three figures are the case of A-Bisphenol polycarbonate.

Figure 6-6 is the case of the untreated substrate surface prior to full fluoropolymer device fabrication. The fluoropolymer is more than 60% peeled away by the mechanical shear force of the cutting blades. Figure 6-7 shows the results from the case of the blanket oxygen treated substrate. In this micrograph, more than 90% of the thin film is

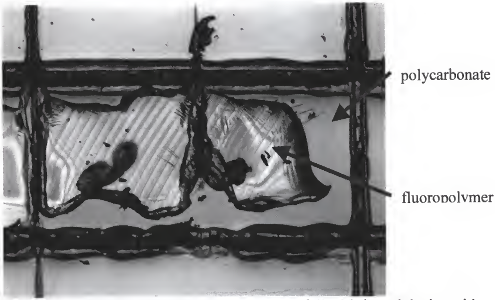

Figure 6-6. Optical micrograph of cross hatch scratch test on fully fabricated device with no substrate surface treatment.

remaining intact on the surface. Slight delamination is seen in areas directly surrounding the blade marks – especially in the corner areas where the blade marks meet. This is a drastic improvement from the case of no treatment which experienced on average more than a 50 % improvement based on total area remaining adhered. This is a nice validation of the results in Chapter 4 which showed much analytical analysis data and some scratch test results on non-fully fabricated devices pointing to a significant improvement in adhesion due to blanket oxygen plasma treatment.

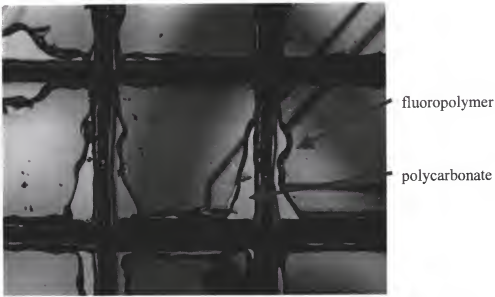

Figure 6-7. Optical micrograph of cross hatch scratch test on fully fabricated device with no substrate surface treatment.

Figure 6-8 shows the results from the case where microfeatures were formed on the surface prior to full device fabrication. In this micrograph, there is full (100%) coverage of the fluoropolymer film following scratch testing. There is no sign of delamination along scratch lines or at the corners between scratch lines as was the case in the blanket oxygen treated sample. This result is characteristic of a outstanding bond quality between the polycarbonate substrate and the fluoropolymer thin film – even following the rigors of damp heat testing.

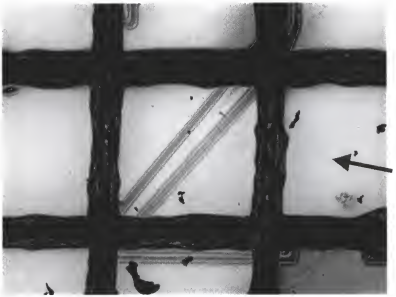

Figure 6-8. Optical micrograph of cross hatch scratch test on fully fabricated device with no substrate surface treatment.

6.3 Discussion

Both real-time and accelerated environmental testing was performed for full devices to evaluate and compare the surface treatment processes using plasma etching. The inspection of optical micrographs shows evidence of delamination exclusively in the case of untreated polycarbonate samples. These samples appear to have failed even before damp heat or temperature cycle testing. In all cases and under all conditions, micrographs show no propagation of the delamination interface between pre and post test results.

In the case of accelerated moisture testing, equation 6.1 may be used to determine the activation energy (*Ea*) associated with the delamination process. In this equation, A

$$K = Ae\frac{-Ea}{kT} \qquad (6.2)$$

is a determinable constant, k is Boltzman's constant, and T is the temperature in Kelvin. If lifetime can be measured for at least two different elevated temperatures, equation 6.1

can be used to determine both A and *Ea*. Equation 6.1 can then be used to calculate lifetime at any other temperature.

Adhesion testing using the cross hatch scratch test was used as a final means to provide a comparison between the treatment methods using the most effective test method available. The untreated sample shows no evidence of acceptable performance. The scratch test removed over 60% of the thin film coverage. The results for the blanket plasma case show a tremendous improvement with only small areas of thin film bond destruction in areas of high shear from the cutting blade. The performance of the microfeature treated substrate is outstanding.

6.4 Summary

These results provide test data showing proof that fluoropolymer waveguide based devices are overwhelmingly capable of mechanically withstanding the environmental test rigors typically required for communications devices. Any level of treatment of the surface by either blanket plasma etch or by microfeature formation allowed devices to pass both damp heat and temperature cycle testing with no failures. Although many further challenges remain to prove the technology fully capable of meeting other aspects of standard industry reliability testing standards, the ability to fabricate highly adherent fluoropolymer thin films on any substrate is a significant accomplishment. For applications requiring the highest level of thin film – surface bonding available, the approach of microfeature formation presents outstanding performance capable of withstanding severe environmental conditions and high levels of shear force.

CHAPTER 7
CONCLUSIONS

Two surface treatment approaches to enhancing the adhesion strength between hydrocarbon polymer and fluoropolymer via the method of Plasma/Reactive-ion etching have been analyzed and evaluated. In addition, devices fabricated under these conditions have been tested under scrutinizing environmental conditions. These methods have been developed through designed experimentation and analytical analysis along with adhesion testing methodologies. These plasma treatment processing methods show results to indicate that they are highly effective treatments which can be used to promote adhesion of thin film cast fluoropolymer on polycarbonate substrate. These treatment methods can be used to enable the production of ultra-low loss polymer waveguide based all optical components for broadband communication as well as other applications which require good adhesion between polymers and fluoropolymer thin films.

7.1 Blanket Oxygen Plasma Treatment

Oxygen plasma treatment for unpatterned surfaces was evaluated for the range of available and acceptable plasma process conditions. Results indicate that there exists a strong relationship between surface area created during the etching process and thin film fluoropolymer adhesion strength. Etching surface roughness evolution was shown to be strongly dependent on total etch depth and a secondary factor in predicting adhesion. Deeper etches produced higher roughness levels. While etching conditions considered to be gentle in nature (40W and 160mtorr) produced very poor adhesion results, conditions considered to be the most aggressive (160W, 40mtor) produced the best adhered films according to scratch test results. The highest level of adhesion was experienced at the condition of 40W, 40mtorr, and 160 seconds - all minimum levels for the factors evaluated. This result suggests that plasma power maximization is not the primary route to achieve the highest levels of enhancement of adhesion. According to AFM results, the optimal treatment results in a near median RMS surface roughness result.

7.2 Etched Microstructure Feature Formation

An alternate approach to thin film adhesion was developed in the evaluation of surface microfeatures on the substrate surface. This approach was evaluated as a solution above and beyond the capabilities of pure surface energy modification by which limitations in the final achievable adhesion strength have been shown to exist. Surface microfeatures of various sizes and aspect ratios were evaluated and analyzed. Optimal size/aspect ratios were shown to exist at which mechanical strength and surface coverage considerations were acceptably balanced. The development of this method for adhesion is an important capability to use when devices are to be exposed to severe environmental conditions or for cases where mechanical methods are heavily utilized in the cutting and packaging of the device.

7.3 Testing of Long Term Performance and Reliability

Testing was performed on a designed experiment matrix evaluating these surface treatments and two types of polycarbonate substrate materials. Standard A-Bisphenol polycarbonate was evaluated as well as a second polycarbonate with slightly different and proprietary chemical structure and higher glass transition temperature. The evaluation of an alternate material was important to assess the relevance of the findings in this work to other substrate compositions. The findings in the work point to the existence of a dependence between substrate composition and adhesion level.

Of the relevant environmental tests for communication devices, the tests of damp heat and temperature cycling were chosen for evaluation. These tests were performed both according to standard specification as well as by using accelerated methods. Testing under standard conditions provided no significant results to draw any conclusions. Devices did not experience delamination for these tests. Under accelerated conditions, the untreated and blanket oxygen treated devices showed eventual failure. The microfeature treated devices did not fail – even under accelerated testing conditions. Accelerated test results were consistent for both substrate types indicating that the blanket oxygen treatment did improve adhesion when compared to the untreated samples. In addition, the alternate, high temperature substrate showed similar results to the standard polycarbonate with somewhat overall higher predicted lifetime but similar trends.

Adhesion scratch testing of fully fabricated optical devices proved extremely valuable in the comparison between treatment methods. Optical micrographs of the scratch test results show a progression of adhesion improvement between untreated, blanket plasma treated, and microfeature treated surfaces.

7.4 Future Work

A novel process for adhesion enhancement via plasma processing for integrated polymer optic components has been demonstrated in microfeature surface formation. The methods of surface activation proposed in this work are primarily solutions dependent on maximized physisorption. In the case of microfeature formation, this physisorption effect is reinforced by combining this with mechanical locking upon casting. The molecular bonding involved is derived exclusively from polar molecular attraction forces – free surface energy. Microfeature structure formation is a complex, but proven approach to ensure a high strength bond. The next step in adhesion promotion resides in the realm of chemisorption where chemical or atomic level bonding is employed. This approach may be attractive in the desire to develop a more simplistic and less costly solution. There are various potential avenues to be investigated to achieve chemisorption using RIE. One such method may involve the plasma alteration/activation of the polycarbonate surface with highly reactive species such as hydroxyl groups and subsequent chemical reaction with the fluoromaterial. Similar work has been published by Gardella et al. in US patent # 4,946,903 where the surface of a fluoropolymer was activated with functionally reactive OH groups [52]. Although this work was performed to activate fluoropolymer materials, it is highly likely that the same general approach would be applicable to other polymers such as polycarbonate. This work will involve unique plasma process gasses such as methanol vapor in combination with H_2O vapor and H_2 gas. The ability to produce chemisorption is a significant breakthrough in the effort to improve adhesion between polymer thin films. Initial work on this approach has produced promising results.

Another area for investigation involves understanding the effect of mechanical shear forces on the properties of adhesion – especially as they relate to long-term reliability. Optical component processing involves the singulation of devices which are fabricated on a circular substrate. This singulation process is typically performed using wafer sawing. Beyond this, singulated die edges to be connected to optical signals require further finishing and smoothing which can be performed using microtoming methods. Both wafer sawing and microtoming induce physical shear force stresses on the substrate/fluorofilm interface. Appreciation of the extent to which these shear force stresses are able to contribute to delamination (especially for long-term reliability) is an important matter for investigation. There are various plasma processing methods which can be developed to possibly reduce or eliminate these effects such as the implementation of a setback border sealing plasma etch.

Other areas of future work involve finding ways to implement these techniques in to various other areas of technology where fluoropolymer films are of value. Such areas include microfluidic devices and fuel cells. The focus on devices or technology with a high level of value added to the end product is important as the cost of the processing and the material can be significant.

APPENDIX A
CROSS HATCH SCRATCH TEST BLADE SPECIFICATION

The following specification was used in the determination of the appropriate cutting blade to be used for the cross hatch adhesion scratch test.

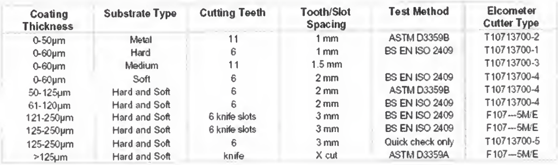

Coating Thickness	Substrate Type	Cutting Teeth	Tooth/Slot Spacing	Test Method	Elcometer Cutter Type
0-50μm	Metal	11	1 mm	ASTM D3359B	T10713700-2
0-60μm	Hard	6	1 mm	BS EN ISO 2409	T10713700-1
0-60μm	Medium	11	1.5 mm		T10713700-3
0-60μm	Soft	6	2 mm	BS EN ISO 2409	T10713700-4
50-125μm	Hard and Soft	6	2 mm	ASTM D3359B	T10713700-4
61-120μm	Hard and Soft	6	2 mm	BS EN ISO 2409	T10713700-4
121-250μm	Hard and Soft	6 knife slots	3 mm	BS EN ISO 2409	F107---5M/E
125-250μm	Hard and Soft	6 knife slots	3 mm	BS EN ISO 2409	F107---5M/E
125-250μm	Hard and Soft	6	3 mm	Quick check only	T10713700-5
>125μm	Hard and Soft	knife	X cut	ASTM D3359A	F107---5M/E

APPENDIX B
BROADBAND CONTACT PHOTOLITHOGRAPHY

The Karl Suss MA-6 system was used to perform the photopatterning required for this study to enable microfeatures in Chapter 5. This information is intended to provide a reference for those interested in the lithography used for this work and to provide further insight in to some of the issues which are unique when patterning on polymer substrates as opposed to silicon/semiconductor wafers.

The system used was a manual aligner with a broadband mercury vapor exposure lamp operating at 400 Watts of power. The photoresist used was Clariant AZ 1505 positive photoresist with PGMEA solvent diluted to achieve a resist thickness of 1μm upon spinning at 2800 rpm. The developing solution used was a standard developer also manufactured by Clariant and sold as 1:1 denoting 1 part developer with 1 part water. A primary constituent of the developer was TMAH (tetramethylammoniumhydroxide).

The exposure system was operated in vacuum contact mode to ensure the best possible contact between the substrate and the mask. This was necessary due to the fact that the substrates were not completely flat with significant thickness variations across the diameter of the surface.

LIST OF REFERENCES

1. F. M. Mims, "Alexander Graham Bell And The Photophone: The Centennial of the Invention of Light-Wave Communications, 1880-1980." Opt. News 6, no. 1 (1980): 8-16.

2. P. McLaughlin, "Why the Copper Vs. Fiber War Is Over," Jul. 2001, Cabling Installation & Maintenance

3. C. Weinstein, "Selecting The Right Transmission Medium; Optical Fiber Is Moving To The Forefront Of Transmission Media Choices Leaving Twisted Copper And Coaxial Cable Behind," Roads & Bridges.

4. J. Palais, *Fiber Optic Communications*, Fourth Edition, p114.

5. C. Schoenberger, "The Greenhouse Effect", Forbes, February 3, 2003. pp54-60.

6. H. Nishihara, *Optical Integrated Circuits*, McGraw-Hill, 1989, pp. 8.

7. D. Bitting, " Polymer Substrates For Polymer Photonic Devices", IMAPS advanced technology workshop on Optoelectronics Device Packaging - presentations and proceedings, 10/7/03.

8. The Photoninc Spectrum Reference Wall Chart, Laurin Publishing, Photonics Spectra, August 2000

9. M. Weber, *Handbook of Optical Materials*, CRC Press, pp. 97.

10. J.T. Yardley, "Organic Thin Films For Waveguiding Nonlinear Optics," 1996, Chapter 11, pp. 654.

11. University of Mississippi, Department of Polymer Science, www.psrc.usm.edu/macrog/ptfe.htm.

12. B. Thomas, "Fluoropolymers: Applications In High Technology Fields" Ph.D. Dissertation, Clemson University, December 14, 2001, Chapter 1.

13. W. Groh, *Makrol. Chemie*, Vol 189, 1998, pp 2861, R. Norwood, *SPIE* 2001.

14. A. Yeniay, R. Gao, K. Takayama, R. Gao, and A. Garito, " Ultra Low Loss Polymer Waveguides," Optical Society of America, OCIS codes:130,3120) Integrated Optical devices, 2003.

15. G. Hougham. *Fluoropolymers 2*, Kluwer Academic/Plenum Publishers. 1999, pp. 60.

16. C. Deng and T. Tsai, "Method for Coating a Metal Cookware," United States Patent # 5545439.

17. M. Sugawara, *Plasma Etching Fundamentals and Applications*, Oxford University Press.

18. TEL Unity Multi Chamber System – Theory of Process, process manual from TEL Corporation, Japan (1997) 3.

19. S. Wolf and R. N. Tauber, *Silicon Processing for the VLSI Era*, Volume 1, Lattice Press, Sunset Beach, CA, 1986

20. H. Nishihara, *Optical Integrated Circuits*, McGraw-Hill, 1989. pp. 184.

21. TEL *Unity Multi Chamber System – Theory of Process*, process manual from TEL Corporation, Japan (1997) 3.

22. P. Zant, *Microchip Fabrication,* McGraw-Hill, Fourth Edition, 2000. pp 273.

23. H. Ko, J. Nah, K. Paik, and Y. Park, "Effects Of The Polymer Residues On Via Contact Resistance After Reactive Ion Etching," Journal of Vacuum Science and Technology B, 20(3), May/Jun 2002.

24. E. Durand, C. Labrugere, A. Tressaud, and M. Renaud, "Surface Fluorination Of Carboxylated Nitrile Butadiene Rubber: An XPS Study," Plasmas and Polymers, Vol.7. No. 4, December 2002.

25. M. Keil et al., "Argon Plasma-Induced Modifications At The Surface Of Polycarbonate Thin Films," Applied Surface Science, 125 (1998), pp. 273-286.

26. G. Houghman et al., *Fluoropolymers 2*, 1999 Kluwer Academic/Plenum Publishers, pp. 342.

27. G. Houghman et al., *Fluoropolymers 2*, 1999 Kluwer Academic/Plenum Publishers, pp. 345.

28. MxP+ Dielectric Etch centura Chamber Manual, June 1996, Chapter 2, pp. 32

29. Digital Instruments Scanning Probe Microscopy Training Notebook, Version 3, 2000, pp. 11.

30. D. Gardner et al., “Recent Research On Contact Angle And Wettability Measurements”, University of Maine, AEWC Presentation.

31. K. Grundke et al., “Contact Angle Measurements Using ADSA And The Determination Of Solid Surface Tensions Of Polymers,” WWW publication (www.ipfdd.de/research/res12/adsa_p.html).

32. L. Feldman and J. Mayer, *Fundamentals of Surface and Thin Film Analysis*, Prentice Hall, 1986, pp. 214.

33. User’s Guide for Spectrum One FTIR Manufactured by Perkin Elmer, Release A, February 2000.

34. HATR Sampling Accessory User’s Guide for Perkin Elmer Instruments, Release B, January 1999.

35. Y. Lee, S. Han, H. Lim, H. Jung, J. Cho, and Y. Kim, “Surface Characterization Of Polymers Modified By keV and MeV Ion Beams,” Journal of Adhesion Science and Technology, Vol 15, No. 9 (2001), pp. 1079-1089.

36. M. Occhiello, M. Morra, and F. Garbassi, “On The Application Of XPS, SIMMS And QCM To Study The Surface Of a CF4/O2 Plasma Treated Polycarbonate,” Applied Science, vol 36 (1989), pp285-295.

37. D. Hegemann, H. Brunner, C. Oehr, “Plasma Treatment Of Polymers For Surface And Adhesion Improvement,” Nuclear Instruments and Methods in Physics Research, Feb 7, 2003.

38. I. Loh, “Plasma Surface Modification In Biomedical Applications,” AST Technical Journal, www.astp.com.

39. S. Ebnesajjad, *Fluoroplastics Vol 2 – Melt Processable Fluoropolymers,* Plastics Design Library, 2003, pp. 14.

40. J. Palmers, “Surface Modification Using Low-Pressure Plsma Technology,” Medical device and Diagnostic Industry, January 2000.

41. W. Callister, *Materials Science and Engineering an Introduction*, John Wiley and Sons, 1997, pp. 804.

42. E. Petrie, *Handbook of Adhesives & Sealants*, McGraw Hill, 1999, pp. 243.

43. N. Agarwal et al., “Roughness Evolution In Polyimide Films During Plasma Etching,” Applied Physics Letters, Vol 78, No 16, April 16, 2001, pp2294-2296.

44. N. Agarwal et al., "Roughness Evolution In Polymide Films During Plasma Etching," Applied Physics Letters, Vol 78, No 16, April 16, 2001.

45. D. Hegemann, H. Brunner, C. Oehr, "Plasma Treatment Of Polymers For Surface And Adhesion Improvement," Nuclear Instruments and Methods in Physics Research B., Feb. 7, 2003.

46. R. Silverstein and F. Webster, "Spectrometric Identification of Organic Compounds," Sixth Edition, pp. 82.

47. R. Gao, A. Garito, J. Chang, D. Bitting, International patent # WO 03/078304 entitled "Optical Polymer Nanocomposite Substrates With Surface Relief Structures,“ Photon-X, Inc., March 14, 2003,

48. N. Agarwal et al., "Roughness Evolution In Polyimide Films During Plasma Etching," Applied Physics Letters, V78, No16, April 16, 2001.

49. N. Agarwal et al., "Roughness Evolution In Polyimide Films During Plasma Etching," Applied Physics Letters, Vol 78, No 16, April 16, 2001, pp. 2294-2296.

50. L. Elada, "The Promise of Polymers," SPIE's OE magazine, May 2002, pp. 26-29.

51. Telecordia Test Specification GR-1312-CORE, "Generic Requirements For OFAs And Proprietary DWDM Systems Reliability Assurance Criteria," Issue 3, April 1999.

52. J. Gardella, T. Vargo, "Oxyfluoropolymers Having Chemically Reactive Surface Functionality And Increased Surface Energies," US Patent #4,946,903, Aug 7, 1990.

BIOGRAPHICAL SKETCH

Donald Stephen Bitting was born in Scranton, PA on February 15, 1974, to Lois (Stephens) and Donald F. Bitting. He moved with his family to Reading, PA in 1988 and graduated form Schuylkill Valley High School in 1992. He attended Albright College while working part-time at AT&T in Reading, PA, and graduated in 1996 with a degree in physics. Out of college, he accepted a full-time position working for Lucent Bell Laboratories in Orlando, Florida, in June of 1996. In this position, he focused on reactive-ion etching (RIE) and was involved in developing etch processes for some of the most advanced silicon CMOS technologies at that time. He quickly developed an expertise in RIE and went on to pursue a graduate education in materials science and engineering at the University of Florida where he met a fellow RIE expert and departmental advisor in Dr. Pearton. He graduated from UF in 1998 with a master's degree under Dr. Pearton.

He went on to work for Lucent Technologies until 2001 when he left his position to go to work as Director of Process Development for a new start-up, Photon-X, in the business of optical communication devices where he was responsible for building and operating a new fabrication facility for producing photonic ICs. During this time, he completed an MBA from Lehigh University.

I certify that I have read this study and that in my opinion it conforms to acceptable standards of scholarly presentation and is fully adequate, in scope and quality, as a dissertation for the degree of Doctor of Philosophy.

Stephen J. Pearton, Chairman
Professor of Materials Science and
Engineering

I certify that I have read this study and that in my opinion it conforms to acceptable standards of scholarly presentation and is fully adequate, in scope and quality, as a dissertation for the degree of Doctor of Philosophy.

Cammy Abernathy
Professor of Materials Science and
Engineering

I certify that I have read this study and that in my opinion it conforms to acceptable standards of scholarly presentation and is fully adequate, in scope and quality, as a dissertation for the degree of Doctor of Philosophy.

Rajiv Singh
Professor of Materials Science and
Engineering

I certify that I have read this study and that in my opinion it conforms to acceptable standards of scholarly presentation and is fully adequate, in scope and quality, as a dissertation for the degree of Doctor of Philosophy.

David Norton
Professor of Materials Science and
Engineering

I certify that I have read this study and that in my opinion it conforms to acceptable standards of scholarly presentation and is fully adequate, in scope and quality, as a dissertation for the degree of Doctor of Philosophy.

Fan Ren

Fan Ren
Professor of Chemical Engineering

This dissertation was submitted to the Graduate Faculty of the College of Engineering and to the Graduate School and was accepted as partial fulfillment of the requirements for the degree of Doctor of Philosophy.

December 2003

Pramod Khargonekar

Pramod Khargonekar
Dean, College of Engineering

Winfred Phillips
Dean, Graduate School